14. Casazza, A. *et al.* Sema3E–Plexin D1 signaling drives human cancer cell invasiveness and metastatic spreading in mice. *J. Clin. Invest.* **120**, 2684–2698 (2010).
This study shows that SEMA3E–plexin D1 interactions are relevant to the malignancies and the metastatic activities of human cancers.
15. Maione, F. *et al.* Semaphorin 3A overcomes cancer hypoxia and metastatic dissemination induced by antiangiogenic treatment in mice. *J. Clin. Invest.* **122**, 1832–1848 (2012).
16. Maione, F. *et al.* Semaphorin 3A is an endogenous angiogenesis inhibitor that blocks tumor growth and normalizes tumor vasculature in transgenic mouse models. *J. Clin. Invest.* **119**, 3356–3372 (2009).
17. Takegahara, N. *et al.* Plexin-A1 and its interaction with DAP12 in immune responses and bone homeostasis. *Nature Cell Biol.* **8**, 615–622 (2006).
This is the first definitive study to show that plexin A1 is indispensable in both immune and skeletal systems.
18. Toyofuku, T. *et al.* Endosomal sorting by semaphorin 4A in retinal pigment epithelium supports photoreceptor survival. *Genes Dev.* **26**, 816–829 (2012).
19. Bougeret, C. *et al.* Increased surface expression of a newly identified 150-kDa dimer early after human T lymphocyte activation. *J. Immunol.* **148**, 318–323 (1992).
20. Kumanogoh, A. *et al.* Identification of CD72 as a lymphocyte receptor for the class IV semaphorin CD100: a novel mechanism for regulating B cell signaling. *Immunity* **13**, 621–631 (2000).
This is the first report to show that semaphorins have crucial roles in the immune system.
21. Shi, W. *et al.* The class IV semaphorin CD100 plays nonredundant roles in the immune system: defective B and T cell activation in CD100-deficient mice. *Immunity* **13**, 633–642 (2000).
This is the first knockout study in mice to show that semaphorins are crucial for immune responses.
22. Kumanogoh, A. *et al.* Class IV semaphorin Sema4A enhances T-cell activation and interacts with Tim-2. *Nature* **419**, 629–633 (2002).
23. Kumanogoh, A. *et al.* Nonredundant roles of Sema4A in the immune system: defective T cell priming and Th1/Th2 regulation in Sema4A-deficient mice. *Immunity* **22**, 305–316 (2005).
24. Suzuki, K. *et al.* Semaphorin 7A initiates T-cell-mediated inflammatory responses through α1β1 integrin. *Nature* **446**, 680–684 (2007).
25. Takamatsu, H. *et al.* Semaphorins guide the entry of dendritic cells into the lymphatics by activating myosin II. *Nature Immunol.* **11**, 594–600 (2010).
This is the first definitive study using imaging analysis to show that plexins are involved in immune cell migration.
26. Suzuki, K., Kumanogoh, A. & Kikutani, H. Semaphorins and their receptors in immune cell interactions. *Nature Immunol.* **9**, 17–23 (2008).
27. Capparuccia, L. & Tamagnone, L. Semaphorin signaling in cancer cells and in cells of the tumor microenvironment — two sides of a coin. *J. Cell Sci.* **122**, 1723–1736 (2009).
28. Nojima, S. *et al.* A point mutation in Semaphorin 4A associates with defective endosomal sorting and causes retinal degeneration. *Nature Commun.* **4**, 1406 (2013).
29. Okuno, T., Nakatsuji, Y. & Kumanogoh, A. The role of immune semaphorins in multiple sclerosis. *FEBS Lett.* **585**, 3829–3835 (2011).
30. Takagi, S. *et al.* The A5 antigen, a candidate for the neuronal recognition molecule, has homologies to complement components and coagulation factors. *Neuron* **7**, 295–307 (1991).
31. He, Z. & Tessier-Lavigne, M. Neuropilin is a receptor for the axonal chemorepellent Semaphorin III. *Cell* **90**, 739–751 (1997).
32. Kolodkin, A. L. *et al.* Neuropilin is a semaphorin III receptor. *Cell* **90**, 753–762 (1997).
33. Takahashi, T. *et al.* Plexin-neuropilin-1 complexes form functional semaphorin-3A receptors. *Cell* **99**, 59–69 (1999).
34. Tamagnone, L. *et al.* Plexins are a large family of receptors for transmembrane, secreted, and GPI-anchored semaphorins in vertebrates. *Cell* **99**, 71–80 (1999).
This study establishes the concept of semaphorin–plexin interactions.
35. Prud'homme, G. J. & Glinka, Y. Neuropilins are multifunctional coreceptors involved in tumor initiation, growth, metastasis and immunity. *Oncotarget* **3**, 921–939 (2012).
36. Soker, S., Takashima, S., Miao, H. Q., Neufeld, G. & Klagsbrun, M. Neuropilin-1 is expressed by endothelial and tumor cells as an isoform-specific receptor for vascular endothelial growth factor. *Cell* **92**, 735–745 (1998).
This study identifies that NRP1 is a receptor for VEGF.
37. Glinka, Y. & Prud'homme, G. J. Neuropilin-1 is a receptor for transforming growth factor β1, activates its latent form, and promotes regulatory T cell activity. *J. Leukoc. Biol.* **84**, 302–310 (2008).
38. Robinson, S. D. *et al.* αvβ3 integrin limits the contribution of neuropilin-1 to vascular endothelial growth factor-induced angiogenesis. *J. Biol. Chem.* **284**, 33966–33981 (2009).
39. Valdembri, D. *et al.* Neuropilin-1/GIPC1 signaling regulates α5β1 integrin traffic and function in endothelial cells. *PLoS Biol.* **7**, e25 (2009).
40. Lanahan, A. *et al.* The neuropilin 1 cytoplasmic domain is required for VEGF-A-dependent arteriogenesis. *Dev. Cell* **25**, 156–168 (2013).
41. Dzionek, A. *et al.* BDCA-2, BDCA-3, and BDCA-4: three markers for distinct subsets of dendritic cells in human peripheral blood. *J. Immunol.* **165**, 6037–6046 (2000).
42. Reizis, B., Bunin, A., Ghosh, H. S., Lewis, K. L. & Sisirak, V. Plasmacytoid dendritic cells: recent progress and open questions. *Annu. Rev. Immunol.* **29**, 163–183 (2011).
43. Grage-Griebenow, E. *et al.* Anti-BDCA-4 (neuropilin-1) antibody can suppress virus-induced IFN-α production of plasmacytoid dendritic cells. *Immunol. Cell Biol.* **85**, 383–390 (2007).
44. Lepelletier, Y. *et al.* Control of human thymocyte migration by neuropilin-1/semaphorin-3A-mediated interactions. *Proc. Natl Acad. Sci. USA* **104**, 5545–5550 (2007).
45. Tordjman, R. *et al.* A neuronal receptor, neuropilin-1, is essential for the initiation of the primary immune response. *Nature Immunol.* **3**, 477–482 (2002).
46. Sarris, M., Andersen, K. G., Randow, F., Mayr, L. & Betz, A. G. Neuropilin-1 expression on regulatory T cells enhances their interactions with dendritic cells during antigen recognition. *Immunity* **28**, 402–413 (2008).
47. Solomon, B. D., Mueller, C., Chae, W. J., Alabanza, L. M. & Bynoe, M. S. Neuropilin-1 attenuates autoreactivity in experimental autoimmune encephalomyelitis. *Proc. Natl Acad. Sci. USA* **108**, 2040–2045 (2011).
48. Battaglia, A. *et al.* Neuropilin-1 expression identifies a subset of regulatory T cells in human lymph nodes that is modulated by preoperative chemoradiation therapy in cervical cancer. *Immunology* **123**, 129–138 (2008).
49. Delgoffe, G. M. *et al.* Stability and function of regulatory T cells is maintained by a neuropilin-1–semaphorin-4a axis. *Nature* **501**, 252–256 (2013).
50. Serini, G. *et al.* Class 3 semaphorins control vascular morphogenesis by inhibiting integrin function. *Nature* **424**, 391–397 (2003).
51. Makino, N. *et al.* Involvement of Sema4A in the progression of experimental autoimmune myocarditis. *FEBS Lett.* **582**, 3935–3940 (2008).
52. Oinuma, I., Ishikawa, Y., Katoh, H. & Negishi, M. The Semaphorin 4D receptor Plexin-B1 is a GTPase activating protein for R-Ras. *Science* **305**, 862–865 (2004).
53. Tamagnone, L. & Mazzone, M. Semaphorin signals on the road of endothelial tip cells. *Dev. Cell* **21**, 189–190 (2011).
54. Barberis, D. *et al.* p190 Rho-GTPase activating protein associates with plexins and it is required for semaphorin signalling. *J. Cell Sci.* **118**, 4689–4700 (2005).
55. Perrot, V., Vazquez-Prado, J. & Gutkind, J. S. Plexin B regulates Rho through the guanine nucleotide exchange factors leukemia-associated Rho GEF (LARG) and PDZ-RhoGEF. *J. Biol. Chem.* **277**, 43115–43120 (2002).
56. Swiercz, J. M., Kuner, R., Behrens, J. & Offermanns, S. Plexin-B1 directly interacts with PDZ-RhoGEF/LARG to regulate RhoA and growth cone morphology. *Neuron* **35**, 51–63 (2002).
57. Terman, J. R., Mao, T., Pasterkamp, R. J., Yu, H. H. & Kolodkin, A. L. MICALs, a family of conserved flavoprotein oxidoreductases, function in plexin-mediated axonal repulsion. *Cell* **109**, 887–900 (2002).
58. Toyofuku, T. *et al.* FARP2 triggers signals for Sema3A-mediated axonal repulsion. *Nature Neurosci.* **8**, 1712–1719 (2005).
59. Takegahara, N. *et al.* Integral roles of a guanine nucleotide exchange factor, FARP2, in osteoclast podosome rearrangements. *FASEB J.* **24**, 4782–4792 (2010).
60. Saito, Y., Oinuma, I., Fujimoto, S. & Negishi, M. Plexin-B1 is a GTPase activating protein for M-Ras, remodelling dendrite morphology. *EMBO Rep.* **10**, 614–621 (2009).
61. Wang, Y. *et al.* Plexins are GTPase-activating proteins for Rap and are activated by induced dimerization. *Sci. Signal.* **5**, ra6 (2012).
62. Giordano, S. *et al.* The semaphorin 4D receptor controls invasive growth by coupling with Met. *Nature Cell Biol.* **4**, 720–724 (2002).
63. Toyofuku, T. *et al.* Dual roles of Sema6D in cardiac morphogenesis through region-specific association of its receptor, Plexin-A1, with off-track and vascular endothelial growth factor receptor type 2. *Genes Dev.* **18**, 435–447 (2004).
64. Wong, A. W. *et al.* CIITA-regulated plexin-A1 affects T-cell-dendritic cell interactions. *Nature Immunol.* **4**, 891–898 (2003).
65. Gu, C. & Giraudo, E. The role of semaphorins and their receptors in vascular development and cancer. *Exp. Cell Res.* **319**, 1306–1316 (2013).
66. Suto, F. *et al.* Interactions between plexin-A2, plexin-A4, and semaphorin 6A control lamina-restricted projection of hippocampal mossy fibers. *Neuron* **53**, 535–547 (2007).
67. Kigel, B., Rabinowicz, N., Varshavsky, A., Kessler, O. & Neufeld, G. Plexin-A4 promotes tumor progression and tumor angiogenesis by enhancement of VEGF and bFGF signaling. *Blood* **118**, 4285–4296 (2011).
68. Roney, K., Holl, E. & Ting, J. Immune plexins and semaphorins: old proteins, new immune functions. *Protein Cell* **4**, 17–26 (2013).
69. Yamamoto, M. *et al.* Plexin-A4 negatively regulates T lymphocyte responses. *Int. Immunol.* **20**, 413–420 (2008).
70. Wen, H., Lei, Y., Eun, S. Y. & Ting, J. P. Plexin-A4–semaphorin 3A signaling is required for Toll-like receptor- and sepsis-induced cytokine storm. *J. Exp. Med.* **207**, 2943–2957 (2010).
71. Tamagnone, L. & Comoglio, P. M. Signalling by semaphorin receptors: cell guidance and beyond. *Trends Cell Biol.* **10**, 377–383 (2000).
72. Deng, S. *et al.* Plexin-B2, but not Plexin-B1, critically modulates neuronal migration and patterning of the developing nervous system *in vivo*. *J. Neurosci.* **27**, 6333–6347 (2007).
73. Artigiani, S. *et al.* Functional regulation of semaphorin receptors by proprotein convertases. *J. Biol. Chem.* **278**, 10094–10101 (2003).
74. Chabbert-de Ponnat, I. *et al.* Soluble CD100 functions on human monocytes and immature dendritic cells require plexin C1 and plexin B1, respectively. *Int. Immunol.* **17**, 439–447 (2005).
75. Granziero, L. *et al.* CD100/Plexin-B1 interactions sustain proliferation and survival of normal and leukemic $CD5^+$ B lymphocytes. *Blood* **101**, 1962–1969 (2003).
76. Smith, E. P. *et al.* Expression of neuroimmune semaphorins 4A and 4D and their receptors in the lung is enhanced by allergen and vascular endothelial growth factor. *BMC Immunol.* **12**, 30 (2011).
77. Li, M. *et al.* Endogenous CD100 promotes glomerular injury and macrophage recruitment in experimental crescentic glomerulonephritis. *Immunology* **128**, 114–122 (2009).
78. Giraudon, P. *et al.* Semaphorin CD100 from activated T lymphocytes induces process extension collapse in oligodendrocytes and death of immature neural cells. *J. Immunol.* **172**, 1246–1255 (2004).
79. Okuno, T. *et al.* Roles of Sema4D–plexin-B1 interactions in the central nervous system for pathogenesis of experimental autoimmune encephalomyelitis. *J. Immunol.* **184**, 1499–1506 (2010).
80. Oinuma, I., Katoh, H., Harada, A. & Negishi, M. Direct interaction of Rnd1 with Plexin-B1 regulates PDZ-RhoGEF-mediated Rho activation by Plexin-B1 and induces cell contraction in COS-7 cells. *J. Biol. Chem.* **278**, 25671–25677 (2003).
81. Basile, J. R., Barac, A., Zhu, T., Guan, K. L. & Gutkind, J. S. Class IV semaphorins promote angiogenesis by stimulating Rho-initiated pathways through plexin-B. *Cancer Res.* **64**, 5212–5224 (2004).
82. Vikis, H. G., Li, W. & Guan, K. L. The plexin-B1/Rac interaction inhibits PAK activation and enhances Sema4D ligand binding. *Genes Dev.* **16**, 836–845 (2002).

83. Holl, E. K. *et al.* Plexin-B2 and Plexin-D1 in dendritic cells: expression and IL-12/IL-23p40 production. *PLoS ONE* **7**, e43333 (2012).
84. Witherden, D. A. *et al.* The CD100 receptor interacts with its plexin B2 ligand to regulate epidermal γδ T cell function. *Immunity* **37**, 314–325 (2012).
85. Pasterkamp, R. J., Peschon, J. J., Spriggs, M. K. & Kolodkin, A. L. Semaphorin 7A promotes axon outgrowth through integrins and MAPKs. *Nature* **424**, 398–405 (2003).
86. Kang, S. *et al.* Intestinal epithelial cell-derived semaphorin 7A negatively regulates development of colitis via αvβ1 integrin. *J. Immunol.* **188**, 1108–1116 (2012).
87. Comeau, M. R. *et al.* A poxvirus-encoded semaphorin induces cytokine production from monocytes and binds to a novel cellular semaphorin receptor, VESPR. *Immunity* **8**, 473–482 (1998).
88. Kang, H. R., Lee, C. G., Homer, R. J. & Elias, J. A. Semaphorin 7A plays a critical role in TGF-β1-induced pulmonary fibrosis. *J. Exp. Med.* **204**, 1083–1093 (2007).
89. Gitler, A. D., Lu, M. M. & Epstein, J. A. PlexinD1 and semaphorin signaling are required in endothelial cells for cardiovascular development. *Dev. Cell* **7**, 107–116 (2004).
90. Toyofuku, T. *et al.* Semaphorin-4A, an activator for T-cell-mediated immunity, suppresses angiogenesis via Plexin-D1. *EMBO J.* **26**, 1373–1384 (2007).
91. Choi, Y. I. *et al.* PlexinD1 glycoprotein controls migration of positively selected thymocytes into the medulla. *Immunity* **29**, 888–898 (2008).
92. Holl, E. K. *et al.* Plexin-D1 is a novel regulator of germinal centers and humoral immune responses. *J. Immunol.* **186**, 5603–5611 (2011).
93. Meda, C. *et al.* Semaphorin 4A exerts a proangiogenic effect by enhancing vascular endothelial growth factor-A expression in macrophages. *J. Immunol.* **188**, 4081–4092 (2012).
94. Goshima, Y., Sasaki, Y., Yamashita, N. & Nakamura, F. Class 3 semaphorins as a therapeutic target. *Expert Opin. Ther. Targets* **16**, 933–944 (2012).
95. Kumanogoh, A. *et al.* Requirement for the lymphocyte semaphorin, CD100, in the induction of antigen-specific T cells and the maturation of dendritic cells. *J. Immunol.* **169**, 1175–1181 (2002).
96. Nakatsuji, Y. *et al.* Elevation of Sema4A implicates Th cell skewing and the efficacy of IFN-β therapy in multiple sclerosis. *J. Immunol.* **188**, 4858–4865 (2012).
97. Ikeda, M., Hosoda, Y., Hirose, S., Okada, Y. & Ikeda, E. Expression of vascular endothelial growth factor isoforms and their receptors Flt-1, KDR, and neuropilin-1 in synovial tissues of rheumatoid arthritis. *J. Pathol.* **191**, 426–433 (2000).
98. Kong, J. S. *et al.* Anti-neuropilin-1 peptide inhibition of synoviocyte survival, angiogenesis, and experimental arthritis. *Arthritis Rheum.* **62**, 179–190 (2010).
99. Catalano, A. The neuroimmune semaphorin-3A reduces inflammation and progression of experimental autoimmune arthritis. *J. Immunol.* **185**, 6373–6383 (2010).
100. Vadasz, Z. *et al.* Semaphorin 3A is a marker for disease activity and a potential immunoregulator in systemic lupus erythematosus. *Arthritis Res. Ther.* **14**, R146 (2012).
101. Vadasz, Z. & Toubi, E. Semaphorin 3A - a marker for disease activity and a potential putative disease-modifying treatment in systemic lupus erythematosus. *Lupus* **21**, 1266–1270 (2012).
102. Yamaguchi, J. *et al.* Semaphorin3A alleviates skin lesions and scratching behavior in NC/Nga mice, an atopic dermatitis model. *J. Invest. Dermatol.* **128**, 2842–2849 (2008).
103. Kou, K. *et al.* Decreased expression of semaphorin-3A, a neurite-collapsing factor, is associated with itch in psoriatic skin. *Acta Derm. Venereol* **92**, 521–528 (2012).
104. Sawaki, H. *et al.* Intranasal administration of semaphorin-3A alleviates sneezing and nasal rubbing in a murine model of allergic rhinitis. *J. Pharmacol. Sci.* **117**, 34–44 (2011).
105. Nkyimbeng-Takwi, E. H. *et al.* Neuroimmune semaphorin 4A downregulates the severity of allergic response. *Mucosal Immunol.* **5**, 409–419 (2012).
106. Morihana, T. *et al.* An inhibitory role for Sema4A in antigen-specific allergic asthma. *J. Clin. Immunol.* **33**, 200–209 (2013).
107. Duran-Struuck, R. *et al.* A novel role for the semaphorin Sema4D in the induction of allo-responses. *Biol. Blood Marrow Transplant.* **13**, 1294–1303 (2007).
108. Adams, R. H., Lohrum, M., Klostermann, A., Betz, H. & Puschel, A. W. The chemorepulsive activity of secreted semaphorins is regulated by furin-dependent proteolytic processing. *EMBO J.* **16**, 6077–6086 (1997).
109. Chen, H., He, Z. & Tessier-Lavigne, M. Axon guidance mechanisms: semaphorins as simultaneous repellents and anti-repellents. *Nature Neurosci.* **1**, 436–439 (1998).
110. Nakamura, F., Tanaka, M., Takahashi, T., Kalb, R. G. & Strittmatter, S. M. Neuropilin-1 extracellular domains mediate semaphorin D/III-induced growth cone collapse. *Neuron* **21**, 1093–1100 (1998).
111. Parker, M. W., Xu, P., Guo, H. F. & Vander Kooi, C. W. Mechanism of selective VEGF-A binding by neuropilin-1 reveals a basis for specific ligand inhibition. *PLoS ONE* **7**, e49177 (2012).
112. Geretti, E., Shimizu, A., Kurschat, P. & Klagsbrun, M. Site-directed mutagenesis in the B-neuropilin-2 domain selectively enhances its affinity to VEGF165, but not to semaphorin 3F. *J. Biol. Chem.* **282**, 25698–25707 (2007).
113. Miao, H. Q. *et al.* Neuropilin-1 mediates collapsin-1/semaphorin III inhibition of endothelial cell motility: functional competition of collapsin-1 and vascular endothelial growth factor-165. *J. Cell Biol.* **146**, 233–242 (1999).
114. Parker, M. W., Guo, H. F., Li, X., Linkugel, A. D. & Vander Kooi, C. W. Function of members of the neuropilin family as essential pleiotropic cell surface receptors. *Biochemistry* **51**, 9437–9446 (2012).
115. Janssen, B. J. *et al.* Neuropilins lock secreted semaphorins onto plexins in a ternary signaling complex. *Nature Struct. Mol. Biol.* **19**, 1293–1299 (2012).
116. Siebold, C. & Jones, E. Y. Structural insights into semaphorins and their receptors. *Semin. Cell Dev. Biol.* **24**, 139–145 (2013).
117. Vadasz, Z. *et al.* The involvement of immune semaphorins and neuropilin-1 in lupus nephritis. *Lupus* **20**, 1466–1473 (2011).
118. Hitomi, Y. *et al.* Human CD72 splicing isoform responsible for resistance to systemic lupus erythematosus regulates serum immunoglobulin level and is localized in endoplasmic reticulum. *BMC Immunol.* **13**, 72 (2012).
119. Takagawa, S. *et al.* Decreased semaphorin3A expression correlates with disease activity and histological features of rheumatoid arthritis. *BMC Musculoskelet Disord.* **14**, 40 (2013).
120. Williams, A. *et al.* Semaphorin 3A and 3F: key players in myelin repair in multiple sclerosis? *Brain* **130**, 2554–2565 (2007).
121. Ieda, M. *et al.* Sema3a maintains normal heart rhythm through sympathetic innervation patterning. *Nature Med.* **13**, 604–612 (2007).
122. Catalano, A. *et al.* Semaphorin-3A is expressed by tumor cells and alters T-cell signal transduction and function. *Blood* **107**, 3321–3329 (2006).
123. Nakagawa, Y. *et al.* Identification of semaphorin 4B as a negative regulator of basophil-mediated immune responses. *J. Immunol.* **186**, 2881–2888 (2011).
124. Gautier, G. *et al.* The class 6 semaphorin SEMA6A is induced by interferon-γ and defines an activation status of langerhans cells observed in pathological situations. *Am. J. Pathol.* **168**, 453–465 (2006).
125. Xie, G. *et al.* Association of granulomatosis with polyangiitis (Wegener's) with HLA-DPB1*04 and SEMA6A gene variants: evidence from genome-wide analysis. *Arthritis Rheum.* **65**, 2457–2468 (2013).
126. Delaire, S. *et al.* Biological activity of soluble CD100. II. Soluble CD100, similarly to H-SemaIII, inhibits immune cell migration. *J. Immunol.* **166**, 4348–4354 (2001).
127. Zhu, L. *et al.* Disruption of SEMA4D ameliorates platelet hypersensitivity in dyslipidemia and confers protection against the development of atherosclerosis. *Arterioscler. Thromb. Vasc. Biol.* **29**, 1039–1045 (2009).
128. Czopik, A. K., Bynoe, M. S., Palm, N., Raine, C. S. & Medzhitov, R. Semaphorin 7A is a negative regulator of T cell responses. *Immunity* **24**, 591–600 (2006).
129. Walzer, T., Galibert, L., Comeau, M. R. & De Smedt, T. Plexin C1 engagement on mouse dendritic cells by viral semaphorin A39R induces actin cytoskeleton rearrangement and inhibits integrin-mediated adhesion and chemokine-induced migration. *J. Immunol.* **174**, 51–59 (2005).

Acknowledgements
We gratefully thank S. Kang, K. Morimoto, S. Nojima and H. Yoshida for help with the figures and tables. This study was supported by research grants from the Ministry of Education, Culture, Sports, Science and Technology of Japan (to A.K. and H. K.), and by the Funding Programs for Core Research for Evolutional Science and Technology (to A.K.).

Competing interests statement
The authors declare no competing financial interests.

DATABASES
ClinicalTrails.gov: http://www.clinicaltrials.gov/NCT01764737

ALL LINKS ARE ACTIVE IN THE ONLINE PDF

Jpn J Radiol (2013) 31:677–684
DOI 10.1007/s11604-013-0235-3

ORIGINAL ARTICLE

Computer-assisted solid lung nodule 3D volumetry on CT: influence of scan mode and iterative reconstruction: a CT phantom study

Adriaan Coenen · Osamu Honda · Eric J. van der Jagt · Noriyuki Tomiyama

Received: 27 May 2013 / Accepted: 31 July 2013 / Published online: 18 August 2013

Abstract
Objective To evaluate the effect of high-resolution scan mode and iterative reconstruction on lung nodule 3D volumetry.
Methods Solid nodules with various sizes (5, 8, 10 and 12 mm) were placed inside a chest phantom. CT images were obtained with various tube currents, scan modes (conventional mode, high-resolution mode) and iterative reconstructions [0, 50 and 100 % blending of adaptive statistical iterative reconstruction (ASiR) and filtered back projection]. The nodule volumes were calculated using semiautomatic software and compared with the assumed volume from the nodules.
Results The mean absolute and relative percentage error improved when using iterative reconstruction especially when using the conventional scan mode; however, this effect was not significant. Significant reduction in volume overestimation was observed when using high-resolution scan mode ($P = 0.011$).
Conclusion The high-resolution mode significantly reduces the volume overestimation of 3D volumetry. Iterative reconstruction shows a reduction in volume overestimation and error margin especially with the conventional scan mode; however, this effect was not significant.

Keywords Pulmonary nodule · 3D volumetry · Phantom · Iterative reconstruction · High-resolution mode · ASiR

A. Coenen · O. Honda · N. Tomiyama
Department of Radiology, Osaka University Graduate School of Medicine, 2-2 Yamadaoka, Suita City, Osaka 565-0871, Japan

A. Coenen
Faculty of Medical Sciences, University of Groningen, Antonius Deusinglaan 1, 9713 AV Groningen, The Netherlands

A. Coenen (✉)
Erasmus MC (Hospital), s-Gravendijkwal 230, 3015 CE Rotterdam, The Netherlands
e-mail: adriaancoenen@gmail.com

E. J. van der Jagt
Department of Radiology, University Medical Center Groningen, Hanzeplein 1, 9713 GZ Groningen, The Netherlands

Introduction

Lung cancer is the most commonly diagnosed form of cancer, with a worldwide incidence of 1.2 million and a mortality of approximately 1.1 million [1]. Early stage lung cancer most commonly presents as a small pulmonary nodule on a CT scan. If the nodule is suspect for malignancy, further evaluation with positron emission tomography (PET) or follow-up with a CT scan is advised. The follow-up CT scan can be used to determine possible nodule growth.

It is reported that the majority of malignant nodules double in volume in 20–400 days [2]. A study by Ashraf et al. [3] shows that volume growth of small lung nodules is associated with lung cancer. This association emphasises the need for reliable volume measurements used to calculated volume growth. Currently, growth of pulmonary nodules is measured using the largest diameters on transverse cross-sectional slices in daily clinical work [4].

Currently, computer-aided 3D volumetry of pulmonary nodules is not used in the daily clinical setting. But it is recognised that computer-aided 3D volumetry has better reliability and reproducibility compared to manual assessment with small interobserver variance. It is also

recognised that some scan or reconstruction parameters affect computer-aided 3D volumetry [5]. Previously studies have investigated the effects of scan and reconstruction parameters such as the tube current, reconstruction kernel and field of view [6, 7].

Recent CT techniques can produce better CT images with a higher spatial resolution and lower image noise. In this study we evaluated the effect of a high-resolution scan mode and iterative reconstruction on 3D volumetry. High-resolution mode is a technique based on garnet detectors. It is capable of an increased number of views per gantry rotation, allowing for an increase in sampling. This increased amount of sampling results in higher spatial resolution and better image quality. Previous publications have described a more detailed technical background and evaluated the effect on image quality [8].

Iterative reconstruction is an image reconstruction algorithm that corrects for random fluctuations in photon measurements [9]. Formerly, iterative reconstruction was used in PET and single-photon CT [10, 11]. The most important role of iterative reconstruction is reducing image noise, which leads to better image quality. The effect of iterative reconstruction on the image noise and quality of CT images has been published previously [12–14]. For this study we used the adaptive statistical iterative reconstruction algorithm (ASiR; GE Healthcare, Waukesha, WI, USA) [9]. The purpose of this study was to clarify the effect of high-resolution mode and iterative reconstruction on computer-aided 3D volumetry.

Materials and methods

Phantom and nodules

The phantom used for this study was the anthropomorphic thoracic phantom Multipurpose Chest Phantom N1 "Lungman" (Kyoto Kagaku Inc., Japan). The phantom measures 43 × 40 × 48 cm in width, length and height. A picture of the phantom is shown in Fig. 1. A network of small structures attached to the heart/mediastinum is designed to mimic bronchial and vascular structures. The phantom does not contain a medium to mimic lung parenchyma and instead is filled with air. We used four spherical nodules with a density of +100 Hounsfield units and diameters of 5, 8, 10 and 12 mm.

The nodules were attached to the phantom using double-sided tape. Each nodule was scanned at 20 different locations, 10 times attached to the pleura and 10 times near vascular structures. The nodules with different sizes were placed at the same locations.

The diameter of each nodule was measured 100 times using a digital vernier calliper (0.01 mm). From the average diameter and the formula $V = (4/3)\pi r^3$, we calculated the assumed volume for each nodule.

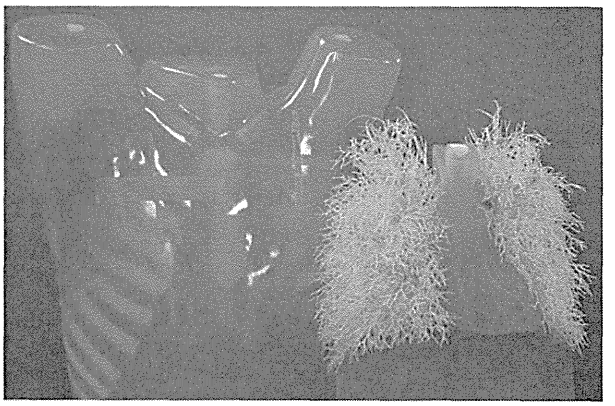

Fig. 1 A picture of the commercially available anthropomorphic thoracic phantom Multipurpose Chest Phantom N1 "Lungman" (Kyoto Kagaku Incorporated, Japan). The phantom is manufactured from urethane to mimics soft tissue and epoxy resins to mimic bone. On the *right side* we see the structure made to mimic the heart/mediastinum, which can be removed through the bottom of the phantom. Attached to the heart/mediastinum is a network of small structures designed to mimic the bronchus and vascular structures

Acquisition and analysis of CT images

For this study all scans were made using a multidetector CT capable of high-resolution mode (Discovery CT750HD, GE Healthcare, Milwaukee, WI, USA). CT scans were performed with either high-resolution or conventional scan mode. For the study we used the following scanning protocol: detector collimation, 64 × 0.625 mm; detector pitch, 0.984; gantry rotation, 0.5 s; matrix size, 512 × 512 pixels; field of view, 20 cm; tube voltage, 120 kVp; tube current for standard dose, 500 mA and for reduced radiation dose 120 mA.

We used the standard and reduced radiation dose to evaluate the effect of high-resolution mode and iterative reconstruction for different CT scanner settings. A field of view of 20 cm for each lung is the clinical standard at the institution where this study took place. Liu et al. [15] found that a minimum tube current necessary for characterisation of ground-glass opacity nodules was 120 mA. Following the ALARA principle we decided to use a tube current of 120 mA for the reduced radiation dose protocol. The CT scanner automatically selects a small or large focal spot size based on the tube voltage, tube current and conventional or high-resolution scan mode. For this study this resulted in a small focal spot size for the reduced radiation dose in both the conventional and high-resolution scan mode. For the normal radiation dose and conventional scan mode, the small focal spot was selected; the normal radiation dose and high-resolution mode resulted in a large

focal spot size. Axial thin-section CT images of 0.625 mm were created using a bone kernel. A high-spatial-frequency algorithm such as bone kernel is preferred as reconstruction kernel for pulmonary nodule volume reconstructions [7, 16]. The software allows blending of the iterative reconstruction with the FBP reconstruction. The amount of blending can be selected from 0 % (FBP image) in increasing steps of 10 % up to 100 % (pure iterative reconstruction image). For this study we used reconstructions of 0, 50 % and 100 % of iterative reconstruction blending.

Automatic 3D volumetry was performed with the software on the workstation (Lung VCAR; GE Healthcare Software). This software segments the pulmonary nodule by combining watershed segmentation and shape-analysis techniques [17]. The software automatically calculates the nodules volume after the centre of the nodule has been manually designated. In total, 960 patterns of the nodules [4 nodules (5, 8, 10 and 12 mm) × 4 scan protocols (high-resolution mode or conventional mode with 500 or 120 mA) × 3 iterative reconstruction techniques settings (0, 50 and 100 %) × 20 locations (10 locations attached to pleura and 10 locations attached to pulmonary vascular)] were analysed with 3D volumetry software.

Statistical analysis

We express our results in absolute percentage error (APE) and relative percentage error (RPE). We calculated the APE and RPE using the following formulas $APE = (|V_{ass.} - V_{cal.}|/V_{ass.}) \times 100$ and $RPE = (V_{cal.} - V_{ass.}/V_{ass.}) \times 100$. In these formulas $V_{ass.}$ is the assumed nodule volume and $V_{cal.}$ is the nodule volume calculated by the 3D volumetry software. The APE is calculated from the absolute difference between the assumed and calculated volume. Both over- and underestimation create a positive APE. In contrast, an underestimation creates a negative RPE. The APE indicates the error margin and the accuracy of the 3D volumetry. The RPE indicates the mean overestimation of the 3D volumetry. We used both the RPE and APE because an overestimation of 3D volumetry has been reported [7]. The use of APE and RPE allowed us to express our results with both accuracy and volume overestimation.

To compare the different scan modes, reconstruction algorithms, radiation doses and nodule sizes, a one-way ANOVA analysis with a post hoc Bonferroni test was used on APE and RPE. To compare pleural and vascular locations, we used an independent *t* test. A sub-analysis was made for high-resolution scan mode, ASiR blending and radiation dose using a paired *t* test. The database was created using the OpenOffice calculator (3.3). Statistical analysis was made with SPSS (17.0). A P value of <0.05 was considered significant.

Results

The assumed nodule volumes obtained from diameter measurements using vernier calliper are summarised in Table 1. An example series of 3D volumetry is shown in Fig. 2.

The results on APE from the 12 different scan and reconstruction patterns are summarised in Fig. 3. The smallest mean APE [5.8 % ± 13.1(SD)] was found in the normal radiation dose, high-resolution mode and 100 % iterative reconstruction blending pattern. The largest mean APE was seen in the normal radiation dose, conventional scan mode and 0 % iterative reconstruction blending (11.5 % ± 39.8). Statistical analysis between the individual patterns showed no significant difference for mean APE or RPE. The mean APE for all 3D volumetry from all patterns was 7.5 % ± 21.3. The mean RPE for all 3D volumetry was 5.6 % ± 21.9.

The effect of nodule size and location

The effects of nodule size on mean APE are summarised in Table 2. APE of the nodule with the 5 mm diameter was 19.1 %, which was significantly higher compared to the nodules with 8, 10 and 12 mm diameters ($P < 0.001$). The difference between the other nodules sizes was not significant. Statistical analysis of RPE showed a similar result.

Table 1 Assumed volume for nodule calculated from 100 diameter measurements

	Assumed nodule volume			
	Mean diameter (mm)	Mean volume (mm^3)	SD from nodule volume	*N*
Nodule 5 mm	5.0	65	1.7	100
Nodule 8 mm	7.9	262	2.4	100
Nodule 10 mm	10.0	516	3.1	100
Nodule 12 mm	12.0	895	7.1	100

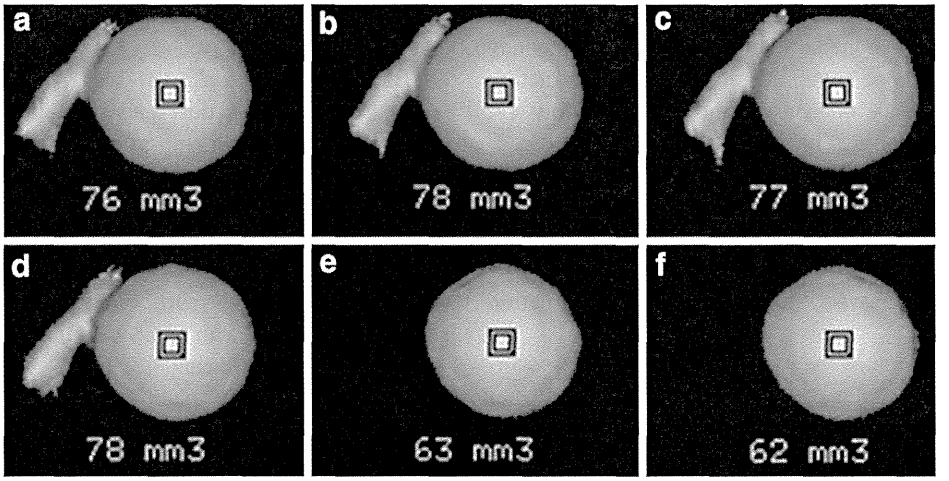

Fig. 2 An example of 3D volumetry from a pulmonary nodule with 5 mm diameter (assumed volume 65 mm^3). The *number* underneath the nodule represents the calculated volume. All reconstructions are made using a tube current of 500 mA. **a** Conventional scan mode 0 % iterative reconstruction; **b** conventional scan mode 50 % iterative reconstruction; **c** conventional scan mode 100 % iterative reconstruction; **d** high-resolution mode 0 % iterative reconstruction; **e** high-resolution mode 50 % iterative reconstruction; **f** high-resolution mode 100 % iterative reconstruction. In this example there is a clear improvement of the 3D volumetry for the high-resolution 50 and 100 % iterative reconstruction. Please note that this figure is added as an illustration of an individual 3D volumetry and does not represent the complete outcome of this study

The APE from nodules attached to the pleura (6.1 % ± 6.9) was significantly lower compared to nodules attached to vascular structures (8.9 % ± 29.3) ($P = 0.044$).

The effect of radiation dose

The effect of reduced radiation dose on the mean APE and RPE is summarised in Fig. 4.

The reduced radiation dose had a lower APE (7.4 % ± 21.5) compared to the normal radiation dose (7.6 % ± 21.2), but this difference was not significant ($P = 0.559$). However, the RPE showed a significant difference between reduced (4.8 % ± 22.2) and normal (6.4 % ± 21.6) radiation dose ($P < 0.001$).

The effect of iterative reconstruction

Analysis of iterative reconstruction blending resulted in a mean APE of 8.8 % ± 27.9, 7.1 % ± 16.4 and 6.6 % ± 17.8 for 0, 50 and 100 % iterative reconstruction, respectively, and statistical analysis showed no significant difference. The results for RPE were similar to those from the APE, with a mean RPE of 7.0 % ± 28.4, 5.2 % ± 17.1 and 4.7 % ± 18.4 for 0, 50 and 100 % iterative reconstruction blending, respectively, and statistical analysis of the RPE also showed no significant difference.

When looking at Fig. 3, we suspect the effect of iterative reconstruction is larger in the reconstructions made with the conventional scan mode. We made a separate paired *t* test to compare the effect of iterative reconstruction within the conventional scan mode for both the normal and reduced radiation setting. This sub-analysis also resulted in a non-significant reduction in APE and RPE.

The effect of high-resolution mode

The effect of high-resolution mode on the mean APE and RPE is shown in Fig. 5. APE of the high-resolution mode (6.6 % ± 17.1) was lower compared to that of the conventional scan mode (8.3 % ± 24.9), but this difference was not significant ($P = 0.066$). However, the mean RPE of high-resolution mode (4.4 % ± 17.8) was significantly ($P < 0.05$) lower than that of the conventional scan mode (6.9 % ± 25.3).

Discussion

Previous studies showed that tube current, reconstruction kernel, slice thickness and nodule size influenced the result on 3D volumetry [6, 7, 15–17]. In this study, the 3D volumetry from all scan and reconstruction patterns resulted in overestimation of the mean calculated volume, especially in small nodules. The 3D volumetry from the 5-mm-diameter nodule was less accurate than those of larger nodules; the effect of increasing inaccuracy with declining nodule size has previously been published [6, 7]. There are two assumptions for this effect. First, the volume error may result from the inaccurate volume measurement of the peripheral part of the nodule by nodule segmentation. If the

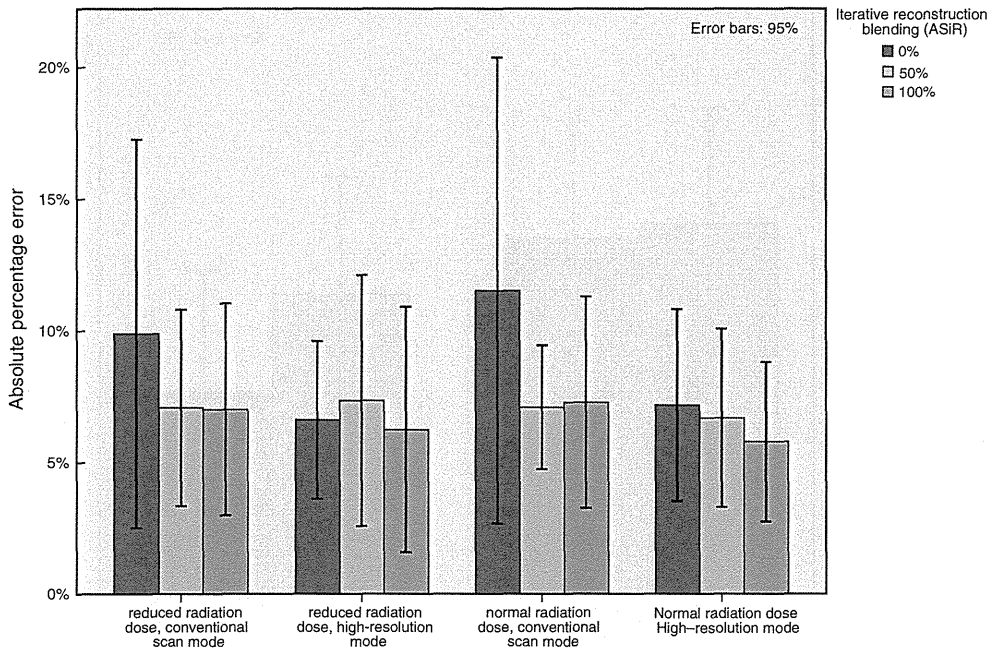

Fig. 3 Absolute percentage error (APE) for the 12 different 3D volumetry patterns. *Each bar* represents the mean APE and is made from 80 3D volumetry reconstructions, resulting in a total of 960 3D volumetry reconstructions. The 95 % error margin is indicated by the *line* on *top* of *each bar*. The difference between these individual patterns is not significant

Table 2 The absolute percentage error for different nodule sizes

Diameter	Mean APE	SD	*N*
Absolute percentage error			
5 mm	19.1	39.7	240
8 mm	4.6	6.6	240
10 mm	3.8	4.3	240
12 mm	2.4	2.4	240
Total	7.5	21.3	960

size of the pulmonary nodule is small, a large part of the nodule will be influenced by the inaccurate segmentation. Therefore, the ratio of the volume error becomes larger in small pulmonary nodules even if the volume error of the small nodule is tiny compared to that of the large nodule. The second assumption was the segmentation error of the nodule from surrounding structures. If the size of the nodule is small, the segmentation of the nodule becomes difficult on 3D volumetry software. In that case, the normal structures such as pulmonary vessels or pleura cannot be removed from the true pulmonary nodule, and the calculated nodule volume contains pulmonary vessels of pleura, which leads to overestimation. In conclusion, we must take care in evaluating small pulmonary nodules by 3D volumetry software.

In our study, there was no significant difference between reduced radiation doses and normal radiation doses in APE, but the RPE in reduced radiation doses was significantly lower than in normal radiation doses. Linning et al. [18] documented that there was no significant difference in APE while there was a significant difference in RPE, and there was substantial underestimation at 30, 60 and 90 mA and substantial overestimation at 120, 150, 180 and 210 mA of tube current on volumetric measurement of ground-glass opacity nodules using a chest phantom. When observing the 3D volumetry from the reduced radiation dose patterns, we saw that the surface was irregular and had numerous small holes in it, giving it a "golf ball"-like appearance. Possibly these surface irregularities occur because of increased noise and decreased spatial resolution, making segmentation of the surface more difficult. A reduced radiation dose may have the effect of making the calculated nodule volume smaller compared to a normal radiation dose.

Surprisingly, a non-significant reduction in error margin and volume overestimation in the 3D volumetry was obtained with iterative reconstruction. We hypothesised that the noise reduction effect of iterative reconstruction contributed to the improvement of accurate volume measurement. Though there was no statistical difference in this study, the mean APE and mean RPE were reduced when using iterative reconstruction. When looking at our data we found the effect of iterative reconstruction to be most prominent in the conventional scan mode. Possibly the increased spatial resolution from the high-resolution mode

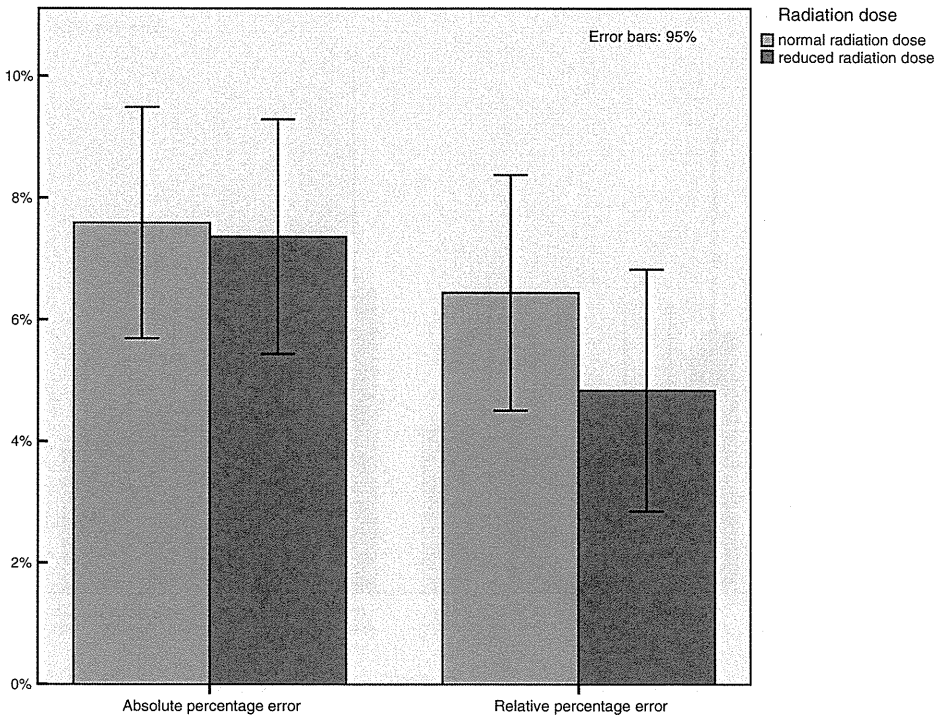

Fig. 4 Absolute and relative percentage error for normal and reduced radiation dose. *Each bar* is made from 480 3D volumetry reconstructions. The 95 % error margin is indicated by the *line* on *top* of *each bar*. The difference in APE is not significant. The RPE of the reduced radiation dose is significantly lower than the RPE from the normal radiation dose

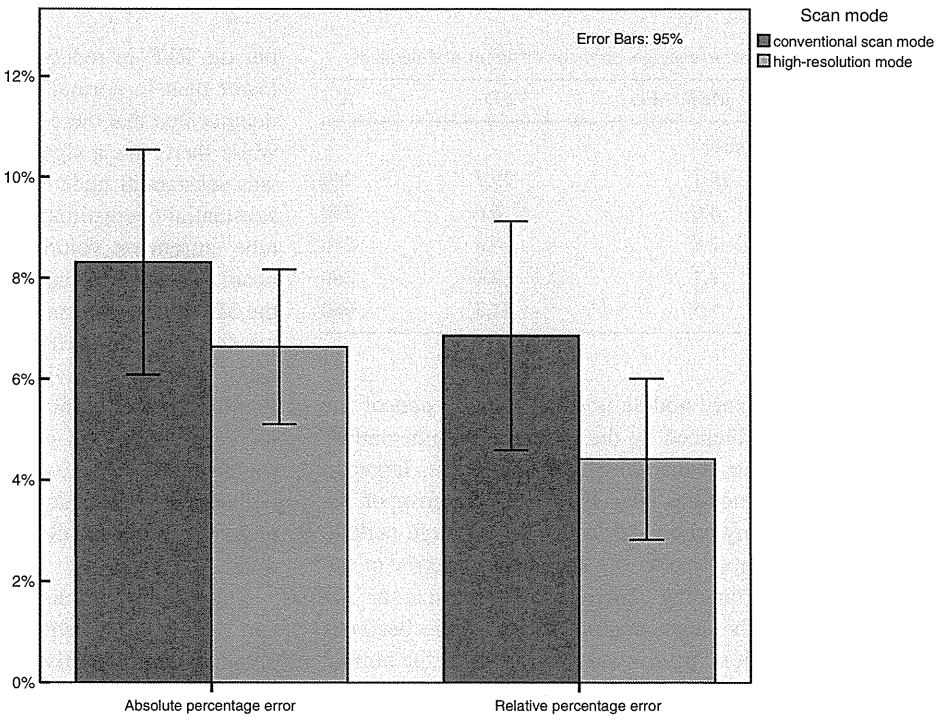

Fig. 5 Absolute and relative percentage error for conventional scan mode and high-resolution scan mode. *Each bar* is made from 480 3D volumetry reconstructions. The difference in APE is not significant ($P = 0.066$); the difference in RPE is significant ($P = 0.011$)

reduces the effect of iterative reconstruction on 3D volumetry. Therefore, we also evaluated the effect of iterative reconstruction in the conventional scan mode; however, this effect was also non-significant. This result may be due to the small sample size, and possibly a larger sample size will result in a significant reduction. When we saw some individual cases, iterative reconstruction resulted in important improvements.

It is important to note that ASiR was used to evaluate the effect of iterative reconstruction on 3D volumetry in

our study. Several other companies have released iterative reconstruction algorithms (AIDR 3D, Toshiba Medical Systems Otawara, Japan; iDose, Philips Healthcare, Best, The Netherlands; SAFIRE, Siemens Medical Systems, Erlangen, Germany), and using a different iterative reconstruction algorithm might result in different outcomes. [19–21].

A study by Willemink et al. evaluated the effect of reduced radiation exposure and iterative reconstruction in a phantom study. They concluded that there was no clinical difference between filtered back projection and iterative reconstruction in nodule volumetry if the diameter of the nodule was 5 mm or larger [22]. In our study, the value of the mean APE and the mean RPE became slightly better by using iterative reconstruction, but there was no statistical difference between filtered back projection and iterative reconstruction as in the study by Willemink et al. Wielpütz et al. [23] recently published a study that evaluates the effect of iterative reconstruction on 3D volumetry in lung nodules placed in ex vivo pig lungs. In this study no significant improvement was found when using iterative reconstruction. It is suggested that the iterative reconstruction may improve the accuracy of the calculated volume in some cases, but the influence of the iterative reconstruction might be limited in 3D nodule volumetry.

Recently, model-based iterative reconstruction has been developed, which has a strong ability to reduce the noise compared to ASiR. Further investigation is needed for model-based iterative reconstruction [24].

The mean APE and RPE of high-resolution mode improved in comparison with those of conventional scan mode. High-resolution mode has more views per gantry rotation than conventional scan mode. Therefore, high-resolution mode can provide more data on CT images, which leads to a higher spatial resolution. Based on this idea we formed the hypothesis that high-resolution mode would increase the accuracy of 3D volumetry. Though high-resolution mode resulted in a non-significant reduction in error margin compared to conventional scan mode, the volume overestimation was significantly reduced with the high-resolution mode. Because of the low but not significant P value in APE, we suspect that this non-significant result in error margin could be due to the small sample size.

In this study, we used only one high-frequency algorithm (bone kernel) for the evaluation of 3D volumetry. In a phantom study, there was no substantial difference in the accuracy of volume estimations across the seven reconstruction kernels including bone and standard algorithm [7]. However, the measured volume with a low-frequency algorithm (standard algorithm) being smaller than that with a high-frequency algorithm (bone algorithm) has been reported in a clinical study [16]. When using high-resolution mode or iterative reconstruction, the margin of the nodule may become more clear, and the influence of the reconstruction algorithm might be reduced on 3D volumetry. If this hypothesis is proven, it would be possible to calculate the doubling time of pulmonary nodules without concern about the reconstruction algorithm.

There are several limitations in our study. First, automatic exposure control (AEC) is used to lower the radiation exposure for the patient in the clinical setting. Our fixed tube current of 500 mA was relatively high compared to the tube current used in clinical settings using AEC [25]. The reduced radiation protocol with a tube current of 120 mA was also relatively high compared to low or ultra-low radiation AEC chest CT scans [26]. In this study, we used these two patterns of tube currency to try to eliminate the effect of a variation in radiation dose. Further investigation to evaluate the effect in ultra-low dose CT is needed in the future. Second, we found small variations in diameter when measuring the nodule diameter using the vernier calliper, resulting in a variation in the assumed nodule volume. Even though this difference was small, it is possible there was an error in the assumed nodule volume. Third, a large focal spot size was automatically selected in the normal radiation dose and high-resolution mode; this could have influenced the outcome of the 3D volumetry. Fourth, the use of a chest phantom results in several study limitations; the physical properties of the phantom are different from those in actual patients; among others, the phantom did not have breathing artefacts. Fifth, the nodules had solid (+100 HU) density and spherical shape in this study, making the segmentation of the nodule easy in 3D volumetry. In clinical practice non-spherical nodules with a lower density (for example, ground-glass nodules) will most likely be more difficult to segment and result in a greater error margin than observed in this phantom study. Sixth, only one software was used in this study for 3D volumetry. Another 3D volumetry software might produce different results, and further investigation is needed.

Conclusion

In this phantom study, the high-resolution mode significantly reduced the volume overestimation of 3D volumetry. We found a reduction in volume overestimation and error margin when using iterative reconstruction especially in the conventional scan mode; however, this effect was not significant.

Acknowledgments We thank the CT technicians of the Osaka University Radiology Department for support with the CT scanner. We thank Dr. J.R. Huizenga and S. Babab MD PhD for their support and work in the International Department for Medical students of the University of Groningen and Osaka University respectively.

Conflict of interest The authors declare that they have no conflict of interest.

References

1. Parkin DM. Global cancer statistics in the year 2000. Lancet Oncol. 2001;2:533–43.
2. Yankelevitz DF, Henschke CI. Does 2-year stability imply that pulmonary nodules are benign? AJR Am J Roentgenol. 1997;168:325–8.
3. Ashraf H, Dirksen A, Loft A, Bertelsen AK, Bach KS, Hansen H, et al. Combined use of positron emission tomography and volume doubling time in lung cancer screening with low-dose CT scanning. Thorax. 2011;66:315–9.
4. Eisenhauer EA, Therasse P, Bogaerts J, Schwartz LH, Sargent D, Ford R, et al. New response evaluation criteria in solid tumours: revised RECIST guideline (version 1.1). Eur J Cancer. 2009;45:228–47.
5. Jennings SG, Winer-Muram HT, Tarver RD, Farber MO, et al. Lung tumor growth: assessment with CT—comparison of diameter and cross-sectional area with volume measurements. Radiology. 2004;231:866–71.
6. Ko JP, Rusinek H, Jacobs EL, Babb JS, Betke M, McGuinness G, et al. Small pulmonary nodules: volume measurement at chest CT—phantom study. Radiology. 2003;228:864–70.
7. Ravenel JG, Leue WM, Nietert PJ, Miller JV, Taylor KK, Silvestri GA, et al. Pulmonary nodule volume: effects of reconstruction parameters on automated measurements—a phantom study. Radiology. 2008;247:400–8.
8. Yanagawa M, Tomiyama N, Honda O, Kikuyama A, Sumikawa H, Inoue A, et al. Multidetector CT of the lung: image quality with garnet-based detectors. Radiology. 2010;255:944–54.
9. Silva AC, Lawder HJ, Hara A, Kujak J, Pavlicek W, et al. Innovations in CT dose reduction strategy: application of the adaptive statistical iterative reconstruction algorithm. AJR Am J Roentgenol. 2010;194:191–9.
10. Knesaurek K, Machac J, Vallabhajosula S, Buchsbaum MS. A new iterative reconstruction technique for attenuation correction in high-resolution positron emission tomography. Eur J Nucl Med. 1996;23:656–61.
11. Wells RG, King MA, Simkin PH, Judy PF, Brill AB, Gifford HC, et al. Comparing filtered backprojection and ordered-subsets expectation maximization for small-lesion detection and localization in 67 Ga SPECT. J Nucl Med. 2000;41:1391–9.
12. Leipsic J, Nguyen G, Brown J, Sin D, Mayo JR. A prospective evaluation of dose reduction and image quality in chest CT using adaptive statistical iterative reconstruction. AJR Am J Roentgenol. 2010;195:1095–9.
13. Yanagawa M, Honda O, Yoshida S, Kikuyama A, Inoue A, Sumikawa H, et al. Adaptive statistical iterative reconstruction technique for pulmonary CT: image quality of the cadaveric lung on standard- and reduced-dose CT. Acad Radiol. 2010;17:1259–66.
14. Prakash P, Kalra MK, Ackman JB, Digumarthy SR, Hsieh J, Do S, et al. Diffuse lung disease: CT of the chest with adaptive statistical iterative reconstruction technique. Radiology. 2010;256:261–9.
15. Liu D, Awai K, Funama Y, Oda S, Nakaura T, Yanaga Y, et al. Identification and characterization of focal ground-glass opacity in the lungs by high-resolution CT using thin-section multidetector helical CT: experimental study using a chest CT phantom. Radiat Med. 2008;26:21–7.
16. Honda O, Johkoh T, Sumikawa H, Inoue A, Tomiyama N, Mihara N, et al. Pulmonary nodules: 3D volumetric measurement with multidetector CT—effect of intravenous contrast medium. Radiology. 2007;245:881–7.
17. Revel MP, Lefort C, Bissery A, Bienvenu M, Aycard L, Chatellier G, et al. Pulmonary nodules: preliminary experience with three-dimensional evaluation. Radiology. 2004;231:459–66.
18. Linning E, Daqing M. Volumetric measurement pulmonary ground-glass opacity nodules with multi-detector CT: effect of various tube current on measurement accuracy—a chest CT phantom study. Acad Radiol. 2009;16:934–9.
19. Yamada Y, Jinzaki M, Hosokawa T, Tanami Y, Sugiura H, Abe T, et al. Dose reduction in chest CT: comparison of the adaptive iterative dose reduction 3D, adaptive iterative dose reduction, and filtered back projection reconstruction techniques. Eur J Radiol. 2012;81(12):4185–95.
20. Noël PB, Fingerle AA, Renger B, Münzel D, Rummeny EJ, Dobritz M. Initial performance characterization of a clinical noise-suppressing reconstruction algorithm for MDCT. AJR Am J Roentgenol. 2011;197:1404–9.
21. Yang WJ, Yan FH, Liu B, Pang LF, Hou L, Zhang H, et al. Can sinogram-affirmed iterative (SAFIRE) reconstruction improve imaging quality on low-dose lung ct screening compared with traditional filtered back projection (FBP) reconstruction? J Comput Assist Tomogr. 2013;37:301–5.
22. Willemink MJ, Leiner T, Budde RP, de Kort FP, Vliegenthart R, van Ooijen PM, et al. Systematic error in lung nodule volumetry: effect of iterative reconstruction versus filtered back projection at different CT parameters. AJR Am J Roentgenol. 2012;199:1241–6.
23. Wielpütz MO, Lederlin M, Wroblewski J, Dinkel J, Eichinger M, Biederer J, et al. CT volumetry of artificial pulmonary nodules using an ex vivo lung phantom: influence of exposure parameters and iterative reconstruction on reproducibility. Eur J Radiol. 2013;. doi:10.1016/j.ejrad.035.
24. Katsura M, Matsuda I, Akahane M, Yasaka K, Hanaoka S, Akai H, et al. Model-based iterative reconstruction technique for ultralow-dose chest CT: comparison of pulmonary nodule detectability with the adaptive statistical iterative reconstruction technique. Invest Radiol. 2013;48:206–12.
25. Mulkens TH, Bellinck P, Baeyaert M, Ghysen D, Van Dijck X, Mussen E, et al. Use of an automatic exposure control mechanism for dose optimization in multi-detector row CT examinations: clinical evaluation. Radiology. 2005;237:213–23.
26. Aberle DR, Berg CD, Black WC, Church TR, Fagerstrom RM, Galen B, et al. The National Lung Screening Trial: overview and study design. Radiology. 2011;258:243–53.

Wilms Tumor Gene (WT1) Peptide–based Cancer Vaccine Combined With Gemcitabine for Patients With Advanced Pancreatic Cancer

Sumiyuki Nishida,† Shigeo Koido,‡ Yutaka Takeda,§ Sadamu Homma,‖ Hideo Komita,‡ Akitaka Takahara,‡ Satoshi Morita,¶ Toshinori Ito,§# Soyoko Morimoto,† Kazuma Hara,** Akihiro Tsuboi,* Yoshihiro Oka,†† Satoru Yanagisawa,‡‡ Yoichi Toyama,‡‡ Masahiro Ikegami,§§ Toru Kitagawa,§ Hidetoshi Eguchi,§ Hiroshi Wada,§ Hiroaki Nagano,§ Jun Nakata,† Yoshiki Nakae,† Naoki Hosen,** Yusuke Oji,‖‖ Toshio Tanaka,††¶¶ Ichiro Kawase,† Atsushi Kumanogoh,†† Junichi Sakamoto,## Yuichiro Doki,§ Masaki Mori,§ Toshifumi Ohkusa,‡ Hisao Tajiri,‡ and Haruo Sugiyama***

Summary: Wilms tumor gene (*WT1*) protein is an attractive target for cancer immunotherapy. We aimed to investigate the feasibility of a combination therapy consisting of gemcitabine and WT1 peptide–based vaccine for patients with advanced pancreatic cancer and to make initial assessments of its clinical efficacy and immunologic response. Thirty-two HLA-A*24:02$^+$ patients with advanced pancreatic cancer were enrolled. Patients received HLA-A*24:02-restricted, modified 9-mer WT1 peptide (3 mg/body) emulsified with Montanide ISA51 adjuvant (WT1 vaccine) intradermally biweekly and gemcitabine (1000 mg/m^2) on days 1, 8, and 15 of a 28-day cycle. This combination therapy was well tolerated. The frequencies of grade 3–4 adverse events for this combination therapy were similar to those for gemcitabine alone. Objective response rate was 20.0% (6/30 evaluable patients). Median survival time and 1-year survival rate were 8.1 months and 29%, respectively. The association between longer survival and positive delayed-type hypersensitivity to WT1 peptide was statistically significant, and longer survivors featured a higher frequency of memory-phenotype WT1-specific cytotoxic T lymphocytes both before and after treatment. WT1 vaccine in combination with gemcitabine was well tolerated for patients with advanced pancreatic cancer. Delayed-type hypersensitivity-positivity to WT1 peptide and a higher frequency of memory-phenotype WT1-specific cytotoxic T lymphocytes could be useful prognostic markers for survival in the combination therapy with gemcitabine and WT1 vaccine. Further clinical investigation is warranted to determine the effectiveness of this combination therapy.

Key Words: Wilms tumor gene (WT1), WT1 peptide vaccine, cancer immunotherapy, pancreatic cancer, gemcitabine

(*J Immunother* 2014;37:105–114)

Pancreatic cancer remains a malignancy with high mortality.[1] Gemcitabine has been the standard first-line treatment for patients with advanced pancreatic cancer, but featured a median overall survival time (MST) of about 6 months and a 1-year overall survival (OS) rate of $\leq$20%.[2] Although many trials of gemcitabine-based combination therapies with cytotoxic or biological agents have been attempted, these therapies, with the exception of erlotinib,[3] have not achieved any survival results superior to those attained with gemcitabine alone.[1] Prognosis of patients with pancreatic cancer thus remains extremely poor, so that novel treatments are urgently needed to improve survival.

Among promising therapeutic strategies, active cancer immunotherapies, such as peptide-based cancer vaccines against tumor-associated antigens (TAAs), which elicit TAA-specific cytotoxic T lymphocytes (CTLs) that eventually eradicate cancer cells, have been and are being developed.[4] However, because their clinical efficacy has been limited,[5,6] several approaches have been tried to improve their efficacy. One approach is the use of combination therapies with certain chemotherapeutic agents, including gemcitabine, which can stimulate the immune system.[7–9] An additional benefit is that chemotherapy makes the tumor cells susceptible to CTL response,[10,11] whereas cancer immunotherapy can sensitize the tumor cells to subsequent chemotherapeutic agents. For this reasons, cancer vaccine in combination with certain chemotherapeutic agents can be expected to exert synergistic effects.

The Wilms tumor gene (*WT1*) is highly expressed in various kinds of malignancies and has been found to perform oncogenic rather than tumor-suppressor functions in tumorigenesis.[12,13] Moreover, both cellular and humoral immune responses against the WT1 protein are naturally elicited in cancer patients, indicating that the *WT1* gene product is actually immunogenic.[14–18] In view of these

Received for publication June 3, 2013; accepted December 16, 2013.
From the Departments of *Cancer Immunotherapy; §Surgery; †Respiratory Medicine, Allergy and Rheumatic Diseases; **Functional Diagnostic Science; ‖‖Cancer Stem Cell Biology; #Complementary and Alternative Medicine; ¶¶Clinical Application of Biologics, Graduate School of Medicine; ††Department of Immunopathology, WPI Immunology Frontier Research Center, Osaka University, Osaka; Departments of ‡Internal Medicine, Division of Gastroenterology and Hepatology; ‖Oncology, Institute of DNA Medicine; Departments of ‡‡Surgery; §§Pathology, The Jikei University School of Medicine, Tokyo; ¶Department of Biostatistics and Epidemiology, Yokohama City University Medical Center, Kanagawa; and ##Department of Young Leaders' Program in Medical Administration, Nagoya University Graduate School of Medicine, Showa-ku, Nagoya, Japan.
S.N. and S.K. contributed equally.
Trial registration ID: UMIN000001187.
Reprints: Haruo Sugiyama, Department of Functional Diagnostic Science, Graduate School of Medicine, Osaka University, 1-7 Yamada-Oka, Suita City, Osaka 565-0871, Japan (e-mail: sugiyama@sahs.med.osaka-u.ac.jp).
Supplemental Digital Content is available for this article. Direct URL citations appear in the printed text and are provided in the HTML and PDF versions of this article on the journal's Website, www.immunotherapy-journal.com.

findings, we and others have been performing clinical studies of the efficacy of WT1 peptide–based immunotherapies for patients, including children, with various kinds of malignancies.[13,19–26]

This report describes a phase 1 clinical study of a WT1 peptide–based cancer vaccine combined with gemcitabine for patients with advanced pancreatic cancer. The main objective of this study was to investigate the feasibility of this combination therapy and to make initial assessments of its clinical efficacy and the immunologic response to WT1 peptide.

MATERIALS AND METHODS

Patient Characteristics

Patients with pathologically or cytologically confirmed, measurable, locally advanced, or metastatic pancreatic adenocarcinoma or with recurrent disease were recruited for this noncomparative, open-label, phase 1 study at 2 centers: Osaka University Hospital and Jikei University Kashiwa Hospital, in Japan. Another major eligibility criterion was HLA-A*24:02 positivity. We chose this phenotype because about 60% of Japanese population had this phonotype. Other eligibility criteria included age of 20 years and older, 75 years and younger, Karnofsky performance status 60%–100%, no previous history of treatment for locally advanced or metastatic disease, a minimum 6-month interval from completion of any previous treatment for recurrent disease, a life expectancy of ≥ 3 months, and adequate organ functions. This study was approved by the ethical review boards of the 2 centers and performed in accordance with the Helsinki Declaration. All patients provided written informed consent.

WT1-Peptide–based Cancer Vaccine (WT1 Vaccine)

A HLA-A*24:02-restricted, modified 9-mer WT1 peptide (mp235; CYTWNQMNL; Peptide Institute Inc., Osaka, Japan) was generated according to the Good Manufacturing Practice Guidelines. In our previous report about the first clinical use of WT1 peptide,[19] the dose-escalation of WT1 peptide from 0.3 to 3.0 mg was designed to decide the recommended dose in combination with the incomplete Freund's adjuvant (Montanide ISA51; Seppic, Paris, France), and 3 mg of WT1 peptide in combination with Montanide ISA51 was decided to be well tolerated. In our present study, we chose WT1 vaccine composed of 3 mg of WT1 peptide and Montanide ISA51 adjuvant. WT1 vaccine was prepared, according to our previous report.[19] WT1 peptide of 3 mg was dissolved in a small volume of dimethyl sulfoxide (DMSO; Sigma, St Louis, MO). The solution was then diluted to 400 μL with 5% glucose and finally emulsified with an equal weight of Montanide ISA51 adjuvant.

Treatment

Gemcitabine was intravenously administered at a dose of 1000 mg/m^2 on days 1, 8, and 15 of a 28-day cycle. WT1 vaccine was intradermally administered at 6 different sites (bilateral upper arms, lower abdomen, and femoral regions) on days 1 and 15 of a 28-day cycle. The initial treatment protocol was planned as 2 courses. Patients without early progressive disease upon the completion of protocol treatment could receive additional treatment until the occurrence of disease progression, unacceptable adverse events, or withdrawal of consent.

Study Assessment

Toxicity was graded using the National Cancer Institute's Common Toxicity Criteria of Adverse Events (CTCAE version 3.0). Dose-limiting toxicity (DLT) was defined as the following adverse events, during the first 2 courses, which were possibly, probably, or definitely related to treatment: grade 4 hematological toxicity lasting >7 days, grade 3 or worse neutropenia accompanied by high fever ($\geq$38°C) or infection (febril neutropenia), and any nonhematological toxicity of grade 3 or worse in other organ systems, including vaccine-injection sites. Biliary tract infection secondary to biliary obstruction was not considered to be a DLT unless it occurred in conjunction with grade ≥ 3 neutropenia. Computed tomography was performed every 4 weeks during the protocol treatment and

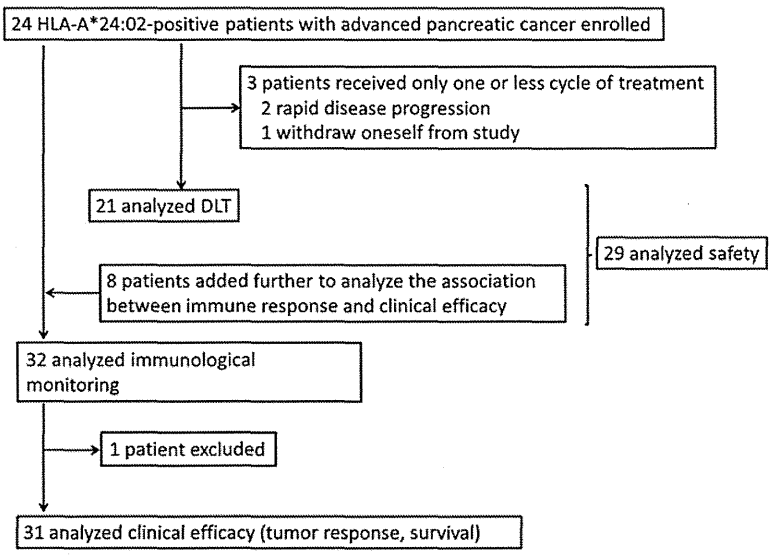

FIGURE 1. Study profile.

every 6–8 weeks during the additional treatment until disease progression, and tumor response was assessed by the investigators according to the Response Evaluation Criteria in Solid Tumors criteria. Stable disease (SD) was defined as a disease that was stable for ≥ 8 weeks after the beginning of treatment. The concentration of the tumor marker carbohydrate antigen 19-9 (CA19-9) was measured at baseline and each course.

WT1-specific Immunologic Assessment

As WT1-specific immunologic assessment, delayed-type hypersensitivity (DTH) to WT1 peptide and the WT1 peptide/HLA-A*24:02 tetramer assay was examined. DTH was examined on day 1 of each course during the protocol treatment and optionally at suitable time during the additional treatment. All DTH tests were performed and measured by the investigators. Briefly, 30 μg of WT1 peptide in saline and saline alone were intradermally injected in the forearm, and the maximum diameter of erythema and other skin reaction, including induration, were measured after 48 hours. DTH-positivity was defined as erythema ≥ 2 mm in diameter, which size was the minimum size measurable with a ruler at the clinical practice.

Peripheral blood (PB) mononuclear cells for WT1 peptide/HLA-A*24:02 tetramer assay were collected on day 1 of each course during the protocol treatment and appropriately during the additional treatment, and cryopreserved until use. The following tetramer and monoclonal antibodies were used: PE-conjugated $WT1_{235}$ tetramer [HLA-A*24:02-restricted natural 9-mer WT1 peptide (CMT WNQMNL)] (MBL, Nagoya, Japan), anti-CD4-FITC, anti-CD16-FITC, anti-CD45RA-APC (BioLegend, San Diego, CA), anti-CD19-FITC, anti-CCR7-PE-Cy7 (BD Pharmingen, San Diego, CA), anti-CD3-PerCP, anti-CD8-APC-Cy7, anti-CD14-FITC (BD Biosciences, San Jose, CA), and anti-CD56-FITC (eBioscience, San Diego, CA). Lineage antigen (CD4, CD14, CD16, CD19, and CD56)-negative, $CD3^-$, $CD8^-$, and $WT1_{235}$ tetramer $^+$ lymphocytes were defined as WT1 tetramer $^+$ $CD3^+$ $CD8^+$ T lymphocytes (WT1-CTLs). Data acquisition were performed on a FACS Aria instrument (BD Biosciences), and data analysis were performed with FACS Diva software (BD Biosciences).

Statistical Analysis

The safety profile constituted the primary end point. A treatment schedule was considered to be acceptable if the probability of developing DLT was estimated to be < 20%. If the estimated probability of DLT occurrence was 10%, the upper limit of the 90% (one-sided) confidence interval (CI) of DLT probability was < 20%, based on the projected sample size of 20 patients. For a more accurate determination of the associations with clinical efficacy and immunologic parameters, in total 32 patients were enrolled (8 patients were further enrolled after the completion of safety assessment with the initial 24 patients as shown in Fig. 1). The secondary end points included objective response, CA19-9 response, defined as a decrease in CA19-9 concentration of at least 50% in the patients with ≥ 100 U/mL of CA19-9 at baseline, progression-free survival defined as time from date of beginning of the treatment to date of disease progression as confirmed by the investigators or death without progression, OS, immunologic responses to WT1 peptide, and correlations between clinical benefit response (CBR)[2] and quality of life (QOL) assessed using by the Functional Assessment of Cancer Therapy-General (FACT-G) measurement system.[27] The nonparametric, Wilcoxon signed-rank test or Mann-Whitney U test was used to calculate P values for change in immune cells because the data were skewed. We judged P values of < 0.01 to be significant. χ^2 test was used to calculate P values for associations between DTH and clinical efficacy. The statistical analyses were performed with SAS for Windows version 9.2 (SAS Institute Inc., Cary, NC). Correlations between CBR and the physical and functional scores based on replies to the FACT-G QOL questionnaire were analyzed with a linear mixed-effects model, for which SAS for Windows release 9.1 (SAS Institute Inc.) was used.

RESULTS

Patient Characteristics

A total of 63 patients with advanced pancreatic cancer, whose median age was 63.0 years old, were screened and checked a phenotype in HLA-A locus. Twenty-two patients failed to enroll in this trial because of lack of HLA-A*24:02 phenotype. A total of 32 HLA-A*24:02 $^+$ patients with advanced pancreatic cancer were finally enrolled in this trial between 2008 and 2010. Of 32 patients, 28 had inoperable advanced pancreatic cancer (6 locally advanced and 22 metastatic diseases), and the remaining 4 had recurrent

TABLE 1. Patients Characteristics at Baseline

Characteristics	N (%)
Age (y)	
Median	60.0
Range	41–75
Sex	
Male	17 (53.1)
Female	15 (46.9)
Karnofsky performance status (%)	
~70	7 (21.9)
80	10 (31.3)
90	12 (37.5)
100	3 (9.4)
Disease extent	
Inoperable advanced disease	28 (87.5)
Locally advanced	6 (18.8)
Metastatic	22 (68.8)
Recurrent disease	4 (12.5)
Local relapse	1 (3.1)
Distant metastasis	3 (9.4)
Primary tumor site	
Head	15 (46.9)
Body/tail	17 (53.1)
Metastatic sites	
Liver	17 (53.1)
Distant lymph node	16 (50.0)
Lung	7 (21.9)
Peritoneum	6 (18.8)
Others*	4 (12.5)
CA19-9 concentration at baseline (U/mL)	
Median	248
Range (U/mL)	< 5–75,050
≤5	3 (9.4)†
6–99	10 (31.3)
100–999	7 (21.9)
1000–9999	5 (15.6)
≥10,000	7 (21.9)

*Other metastatic sites included bone, ovary, or adrenal gland.
†All patients had the Lewis blood group-negative phenotype.
CA19-9 indicates carbohydrate antigen 19-9.

disease. Table 1 summarizes the patient baseline characteristics. Three patients did not complete the first 2 courses of treatment: 2 patients showed rapid disease progression, and 1 refused to continue the treatment. It was determined by the supervising Data Safety and Monitoring Board that the elimination of these cases was unlikely to be or was not related to the protocol treatment. Of the initial 24 patients, 21 could thus to be used for assessment of DLT, 29 of all 32 patients for assessment of adverse events (Fig. 1).

Safety

Administration of WT1 vaccine in combination with gemcitabine was well tolerated. All adverse events are listed in Table 2. The initial assessment of safety for 21 patients found that a grade 4 central nervous system cerebrovascular ischemia considered to be a DLT had occurred in 1 patient. The most commonly reported adverse event was skin toxicity related to WT1 vaccine. All patients developed grade 1 or 2 skin reactions with swelling, redness, erythema, and induration with or without involvement of small vesicles at the local vaccine-injection sites. Hematological abnormalities were similar to those observed with the administration of gemcitabine alone, and none of the patients developed DLTs associated with hematological abnormalities or febril neutropenia. Eight grade 3 nonhematological adverse events (1 instance of hyponatremia and 7 hepatobiliary/pancreas infections) were detected and attributed to complications associated with disease progression or biliary obstruction. Other major nonhematological adverse events included grade 1 or 2 skin rash, anorexia, nausea, and fever, all of which were previously reported as major adverse events associated with gemcitabine. Hepatic transaminase elevation was principally related to disease progression and/or hepatobiliary infection. Except for local skin reactions, none of the patients experienced adverse events considered to be related to WT1 vaccination.

Clinical Response and Survival Analysis

The clinical efficacy results for all 32 patients are summarized in Table 3. Two patients were excluded from some of these analyses. One patient, who had followed a satisfactory and interesting treatment course and finally undergone a surgical resection (Supplementary Figure 1, Supplemental Digital Content 1, http://links.lww.com/JIT/A317 and Table 3), was excluded from the evaluations of response and survival because the diagnosis of pancreatic cancer could not be pathologically confirmed due to the lack of viable tumor cells in the resected specimens. The other patient was excluded from the evaluation of response because of withdrawal of consent before the first evaluation. Thus, of the total of 32 patients, 30 could be used to evaluate response to treatment and 31 to assess survival. Six of 30 patients (20.0%) reached partial response (PR), and 16 of them (53.3%) showed SD at least for ≥ 8 weeks (Table 3). Median progression-free survival was 4.2 months (95% CI, 3.6–4.6) (Fig. 2A) and MST was 8.1 months (95% CI, 6.3–10.0) (Fig. 2B). Six-month and 1-year OS rates were 71.0% (95% CI, 54.9–87.1) and 29.0% (95% CI, 12.9–45.1), respectively (Fig. 2B).

Ten of 19 patients with ≥ 100 U/mL of CA19-9 at baseline (52.6%) showed a decrease in CA19-9 serum concentration of at least 50% (Table 3).

TABLE 2. Adverse Events Reported in 29 Patients who Completed the First 2 Courses of Treatment

	Grades				N (%)		
	1	2	3	4	Any Grade (N = 29)	Grade 3 or 4 (N = 29)	DLT (N = 21)
Hematological abnormalities							
Neutropenia	3	6	13	0	22 (75.9)	13 (44.8)	0 (0.0)
Leukocytopenia	4	12	8	0	24 (82.8)	8 (27.6)	0 (0.0)
Lymphopenia	3	12	8	0	23 (79.3)	8 (27.6)	0 (0.0)
Anemia	6	15	2	0	23 (79.3)	2 (6.9)	0 (0.0)
Thrombocytopenia	15	6	1	0	22 (75.9)	1 (3.4)	0 (0.0)
Nonhematological events							
CNS ischemia	0	0	1	0	1 (3.4)	1 (3.4)	1 (4.8)
Hepatobiliary tract infection with normal ANC	0	1	7	0	8 (27.6)	7 (24.1)	0 (0.0)
Hyponatremia	3	0	1	0	4 (13.8)	1 (3.4)	0 (0.0)
Hypoalubminemia	9	4	0	0	13 (44.8)	0 (0.0)	0 (0.0)
Alanine aminotransferase	9	4	0	0	13 (44.8)	0 (0.0)	0 (0.0)
Aspartate aminotransferase	10	1	0	0	11 (37.9)	0 (0.0)	0 (0.0)
Bilirubin	2	4	0	0	6 (20.7)	0 (0.0)	0 (0.0)
Hyperkalemia	3	0	0	0	3 (10.3)	0 (0.0)	0 (0.0)
Hemorrhage in urinary tracts	2	1	0	0	3 (10.3)	0 (0.0)	0 (0.0)
Proteinuria	2	0	0	0	2 (6.9)	0 (0.0)	0 (0.0)
Hypokalemia	1	0	0	0	1 (3.4)	0 (0.0)	0 (0.0)
Anorexia	9	0	0	0	9 (31.0)	0 (0.0)	0 (0.0)
Rush*	5	3	0	0	8 (27.6)	0 (0.0)	0 (0.0)
Fever	6	1	0	0	7 (24.1)	0 (0.0)	0 (0.0)
Nausea	7	0	0	0	7 (24.1)	0 (0.0)	0 (0.0)
Diarrhea	2	1	0	0	3 (10.3)	0 (0.0)	0 (0.0)

Adverse events were graded using the National Cancer Institute Common Toxicity Criteria of Adverse Events (CTCAE version 3.0).
*Exclude skin reaction at WT1 vaccine-injection sites.
ANC indicates absolute neutrophil count; CNS, central nervous system; DLT, dose-limiting toxicity.

Correlations between CBR and either physical or functional scores assessed with the FACT-G QOL questionnaire were analyzed. For assessment of CBR, 16 of the initial 24 patients (66.7%) could be used. Nine (56.3%) of these patients (3 with PR, 5 with SD, and 1 with progressive disease) were classified as CBR responders (data not shown). CBR responders showed improvement in physical and functional scores during the first 2 courses, whereas both scores for CBR nonresponders tended to become worse (Supplementary Figure 2, Supplmental Digital Content 2, http://links.lww.com/JIT/A318).

WT1-specific Immune Response

Exploratory analyses of the immune response consisted of assessment of DTH to WT1 peptide and WT1 tetramer$^+$ CD3$^+$ CD8$^+$ T lymphocytes (WT1-CTLs) in PB of all 32 patients. All patients were DTH-negative at baseline, but 31 were at least once assessed as DTH after WT1 vaccination and 18 patients (58.1%) showed DTH-positivity, all of which conversion was detected during the protocol treatment. All of the DTH-positive patients showed at least ≥ 4 mm diameter of erythema, which was a length that was easy enough to measure. Next, for evaluation of associations between survival and DTH, the patients were classified into 4 groups according to survival time: Superior (>12 mo), good (8–12 mo), moderate (4–8 mo), and poor ($\leq$4 mo) responders. These categories were based on the following findings: (i) MST for best supportive care only is no more than 3–4 months[1]; (ii) MST of our patients was 8.1 months; and (iii) survival time of >12 months generally indicates that the treatment has been beneficial. DTH-positivity of superior and good responders was 68.7% (11/16), whereas that of poor responders was 0% (0/7). The association between DTH-positivity and longer survival time was statistically significant

TABLE 3. Summary of Clinical Efficacy Results

	All Patients	DTH Positive	DTH Negative
Best overall response [N (%)]			
Complete response	0 (0.0)	0 (0.0)	0 (0.0)
Partial response	6 (20.0)	3 (17.6)	3 (23.1)
Stable disease*	16 (53.3)	12 (70.6)	4 (30.8)
Progressive disease	8 (26.7)	2 (11.8)	6 (46.2)
Excluded	1†	1	0
Not evaluable	1		
CA19-9 response (≥100 U/mL at baseline)	N = 19	N = 11	N = 7
Positive‡ [N (%)]	10 (52.6)	7 (63.6)	3 (42.9)
PFS	N = 31	N = 17	N = 13
Range (d)	21–1504 +	55–1504 +	21–373
Median PFS (mo)	4.2 (1.1–7.4)	5.4 (2.6–8.2)	2.9 (−1.6 to 7.1)
3-mo PFS (%)	67 (50–84)	82 (64–100)	46 (9–73)
OS	N = 31	N = 17	N = 13
Range (d)	30–1504 +	154–1504 +	30–443
Median OS (mo)	8.1 (6.3–10.0)	10.9 (1.2–20.7)	3.9 (−3.0 to 10.7)
6-mo OS (%)	71 (55–87)	88 (73–104)	46 (19–73)
12-mo OS (%)	29 (13–45)	47 (18–65)	7.7 (−6.8 to 22)

(): 95% CI.

*Stable disease conformation is determined at least for ≥ 8 weeks.

†This patient was reached partial response after 3 courses of treatment, and finally underwent the surgical resection. This patient was excluded the analysis of clinical response, PFS, and OS.

‡"Positive" CA19-9 response is defined as a $\geq$50% decrease in CA19-9 concentration after treatment.

CA19-9 indicates carbohydrate antigen 19-9; CI, confidence interval; DTH, delayed-type hypersensitivity; OS, overall survival; PFS, progression-free survival.

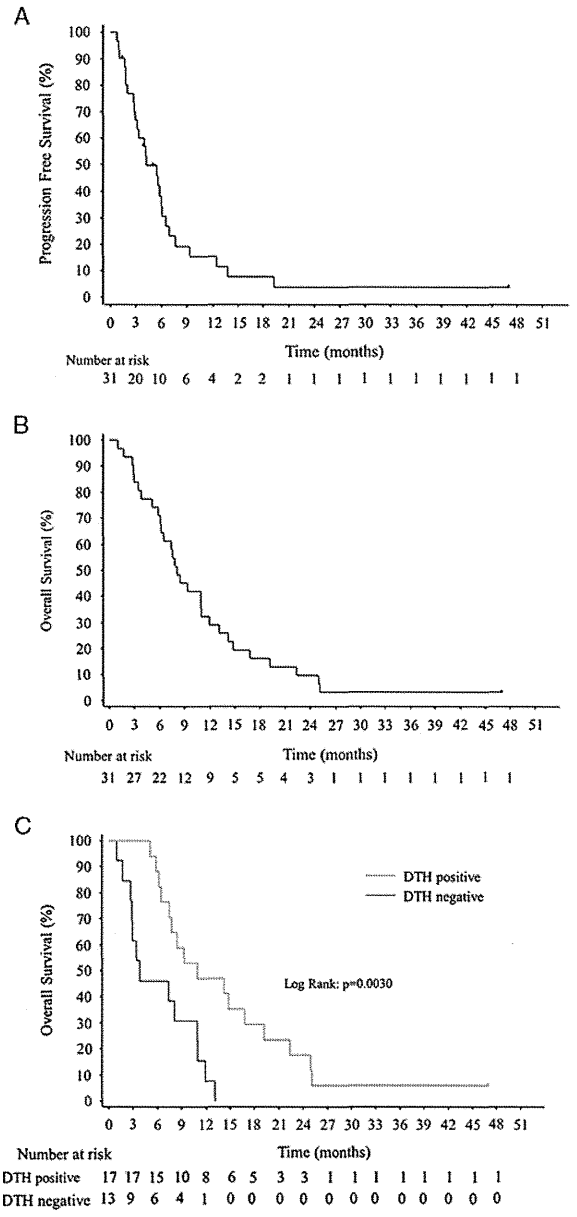

FIGURE 2. Kaplan-Meier survival curves. A, Progression-free survival (N = 31). B, Overall survival (N = 31). C, Overall survival in DTH-positive (gray line) or DTH-negative patients (black line). DTH indicates delayed-type hypersensitivity.

($\chi^2 = 15.908$, $P = 0.0012$) (Table 4). Therefore, survival was retrospectively reanalyzed in terms of DTH-positivity or DTH-negativity. MST was 3.9 and 10.9 months for DTH-negative (N = 13) and DTH-positive (N = 17) patients, respectively, with a statistically significant difference ($P = 0.0030$) (Fig. 2C and Table 3).

The number of WT1-CTLs and the percentages of naive ($CD45RA^+CCR7^+$), memory ($CD45RA^-CCR7^+$ and $CD45RA^-CCR7^-$), and effector ($CD45RA^+CCR7^-$) phenotypes in WT1-CTLs did not show any significant changes during the protocol treatment by the analysis using all patients (Supplementary Table 1, Supplemental Digital Content 3, http://links.lww.com/JIT/A319 and Supplementary Table 2, Supplemental Digital Content 4, http://links.lww.com/JIT/A320). Next, these immunologic parameters were compared between patients showing DTH-positivity and DTH-negativity. The difference in the number of WT1-CTLs was not statistically significant (Supplementary Table 1, Supplemental Digital Content 3, http://links.lww.com/JIT/A319). Phenotype analysis of WT1-CTLs showed that the percentage of naive-phenotype was higher in DTH-positive than in DTH-negative patients at baseline (Fig. 3A). After treatment, DTH-positive patients showed a significantly higher percentage of memory-phenotype and consequently a lower percentage of effector-phenotype WT1-CTLs than did their DTH-negative counterparts (Fig. 3A and Supplementary Table 2, Supplemental Digital Content 4, http://links.lww.com/JIT/A320). Furthermore, the percentage of memory-phenotype WT1-CTLs for the superior responders seemed to be relatively higher than that of effector-phenotype WT1-CTLs (Fig. 3B), whereas this tendency was quite the opposite for the poor responders (Fig. 3B and Supplementary Table 3, Supplemental Digital Content 5, http://links.lww.com/JIT/A321).

Case Report

A 44-year-old male with a locally advanced pancreatic head cancer (T4N1M0; stage III) received WT1 vaccine in combination with gemcitabine, and achieved PR (Fig. 4A). Five months after the beginning of the treatment, this patient underwent a complete surgical resection. Histopathologic examination of the resected specimen showed an invasive ductal adenocarcinoma with mononuclear cell infiltration around the cancer region and moderate to severe fibrotic change (Fig. 4B). This patient proved to be positive for DTH to WT1 peptide after 1 treatment course (Fig. 4C). The number of WT1-CTLs transiently decreased during the first 2–3 treatment courses but subsequently increased again, while the percentage of memory-phenotype WT1-CTLs remained high during the treatment courses (Fig. 4C). Of note, the percentage of WT1-CTLs in the tumor-infiltrating $CD3^+CD8^+$ T lymphocytes was 2.48%, which was about 6 times higher than that in PB (0.39%) (Fig. 4D). This patient had been receiving monthly administration of WT1 vaccine in combination with gemcitabine for 3 years and has maintained a Karnofsky performance status of 100% with no evidence of disease recurrence.

DISCUSSION

This study was designed with a DLT target rate of 10% during the first 2 treatment courses, but only one of the 21 initial evaluable patients (4.8%) actually experienced DLT. These results confirmed that WT1 vaccine in combination with gemcitabine is acceptable for patients with advanced pancreatic cancer. Cerebrovascular ischemia, reported here as a DLT, could be also caused by pancreatic cancer itself and/or the administration of gemcitabine, both of which are sometimes associated with a high risk of developing thrombotic disease.[28,29] Therefore, this adverse event was considered to be multifactorial and judged to be "possibly" related to treatment.

Except for skin reactions at the local injection sites, the toxicity profiles of WT1 vaccine in combination with gemcitabine were consistently similar to those of gemcitabine alone. As the *WT1* gene is physiologically expressed in hematopoietic progenitor cells,[13] damage to hematopoiesis is one of the major concerns in WT1-peptide–based immunotherapy. The incidence of hematological adverse events in our study, however, was similar to that observed for treatment with gemcitabine alone,[30] and these events were easily managed and reversible. These findings suggest that WT1 vaccine does not synergistically intensify hematological adverse events associated with gemcitabine. It seems unlikely that WT1-specific CTLs elicited by WT1 vaccine might damage normal WT1-expressing hematopoietic progenitor cells as well as WT-expressing tumor cells, as following reasons. First, in the previous clinical studies, we and others reported that WT1-specifc CTLs elicited by WT1 vaccine decreased WT1-expressing leukemia cells and suppressed the disease progression of WT-expression cancer cells, but not significantly damaged normal hematopoiesis.[19,23–26] Second, it was demonstrated that, using mice in vivo experiments, WT1-targetting immunotherapy gave damage to tumor cells, but not WT1-expressing normal tissue, including hematopoietic cells.[31,32] The reason why the normal WT1-expressing hematopoietic cells are able to escape from the attack by WT1-specific CTLs is not well known. Further investigations should be required to address this issue.

The clinical efficacy of treatment with WT1 vaccine in combination with gemcitabine, especially in terms of survival, seemed to be better than of that with gemcitabine alone.[1,2] About half of patients who had been induced WT1-specific immunity after vaccination showed better clinical outcome with 12 months or longer survival time, suggesting additional or synergistic effects of WT1 vaccine in combination with gemcitabine. Furthermore, the former contributed to pain relief and thus to improvement of QOL. Recently, the result of the phase III study of gemcitabine plus S-1, S-1 alone, or gemcitabine alone in patients with locally advanced and metastatic pancreatic cancer (GEST study) conducted in Japan and Taiwan between 2007 and 2009 has been reported.[33] Median OS and OS rate at 12

TABLE 4. Association Between DTH and Survival

	Overall Survival				
	>12 mo (Superior)	≤12, >8 mo (Good)	≤8, >4 mo (Moderate)	≤4 mo (Poor)	Total
DTH positive	8*	3	6	0	17*
DTH negative	1	4	1	7	13
Total	9	7	7	7	30

$\chi^2 = 15.908$, $P = 0.0012$.
*One patient was excluded from this analysis.
DTH indicates delayed-type hypersensitivity.

months in the gemcitabine alone group were 8.8 months and 35.4%, respectively. These results seemed a little better than those in our study. One reason for this may be the difference in the proportion of the patients with the locally advanced pancreatic cancer, in which survival data were apparently much better than those in metastatic ones. In our study, this proportion was 18.8%, which was lower than that in GEST study (23.8%). The other reason may be PS at baseline, which was also one of the important prognostic factors. The proportion of the patients with ECOG-PS 0, 1, and 2 at baseline in our study were 46.9%, 31.3%, and 21.9%, respectively, whereas those in GEST study were 65.3%, 34.7%, and 0.0%, respectively. It is apparent that our patients are predicted to worse prognosis than those in GEST study. Despite lower proportion of locally advanced stage and worse PS, however, the survival data gained from the patients with DTH-positivity seemed to be better than those in GEST study. These results suggested additional or synergistic effects of WT1 vaccine. Although the number of patients in our present study was too small to reach any

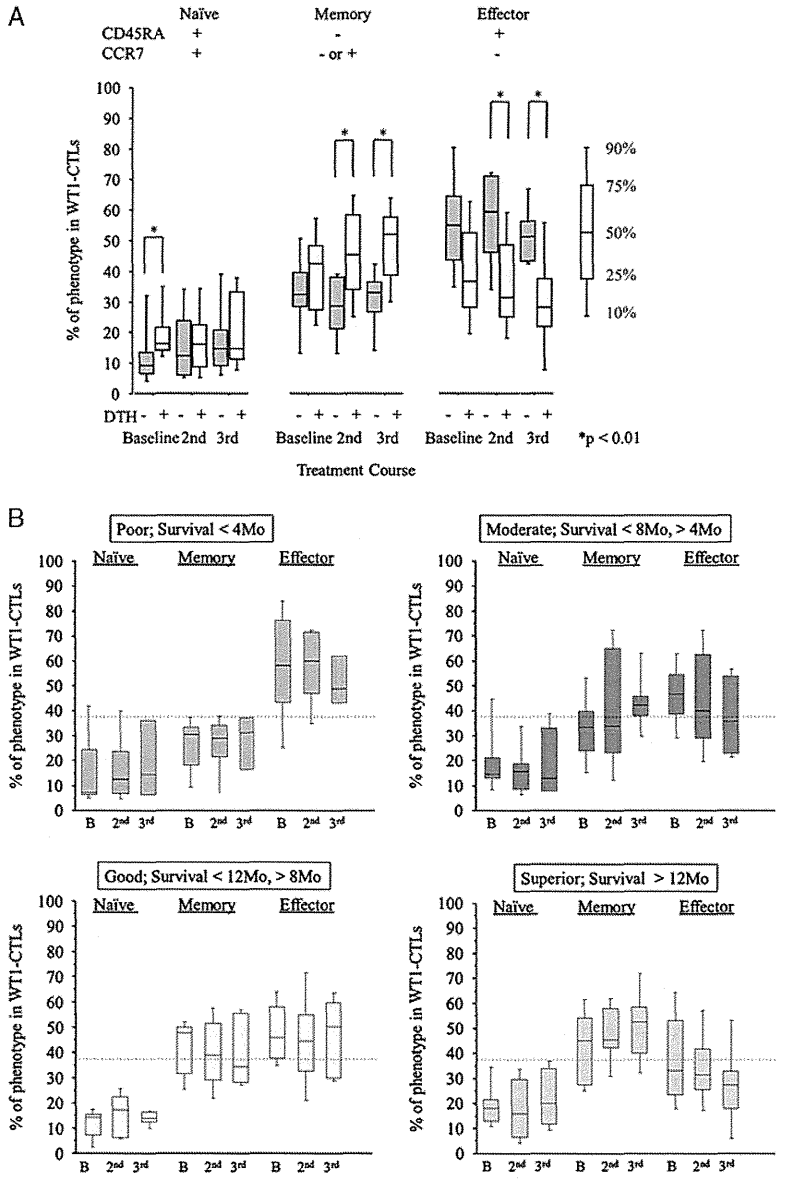

FIGURE 3. Analysis of WT1-specfic immune response. A, Immunologic monitoring of the phenotype analysis of WT1 tetramer$^+$ CD3$^+$CD8$^+$ T lymphocytes (WT1-CTLs) in DTH-positive (light gray columns) and DTH-negative patients (dark gray columns). B, Immunologic monitoring of the phenotype analysis of WT1 tetramer$^+$CD3$^+$CD8$^+$ T lymphocytes (WT1-CTLs) in the patients of 4 groups classified according to overall survival time. The broken line represents the median percentage of memory-phenotype WT1-CTLs at baseline for all patients. WT1 tetramer = PE-conjugated $WT1_{235}$ tetramer [HLA-A*24:02-restricted natural 9-mer WT1 peptide (CMTWNQMNL)], naive (CD45RA$^+$CCR7$^+$), memory (CD45RA-CCR7$^+$ or CD45RA-CCR7$^-$), and effector (CD45RA$^+$CCR7$^-$). 2nd indicates day 1 in the second course; 3rd, day 1 in the third course; B, baseline; DTH, delayed-type hypersensitivity.

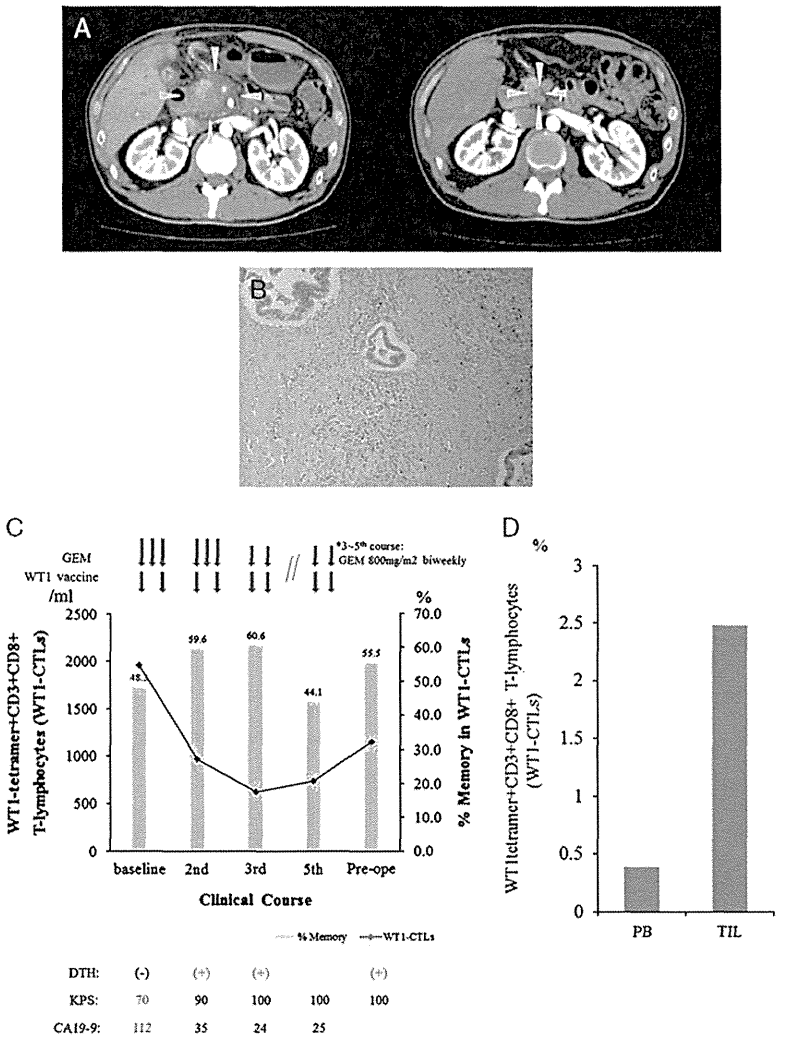

FIGURE 4. Clinical course and immunologic monitoring of 1 patient. A, Abdominal computed tomography (CT) scan before and after treatment. Left: CT scan at baseline showed a large hypodense lesion in the head of the pancreas, which had also invaded the supramesenteric artery and portal vein. Right: 5 months after treatment (before operation), a follow-up CT scan showed >80% regression of the primary lesion. Gray arrows shows primary lesion of pancreas. B, Microscopic findings of the resected specimen (hematoxylin-eosin stain). C, Clinical course and immunologic monitoring. The black line represents the absolute number of WT1 tetramer$^+$CD3$^+$CD8$^+$ T lymphocytes (WT1-CTLs), and the gray column represents the percentage of memory-phenotype WT1-CTLs. D, Percentages of WT1-CTLs in the peripheral blood (PB) and tumor-infiltrating lymphocytes (TIL). CA19-9 indicates carbohydrate antigen 19-9; CTLs, cytotoxic T lymphocytes; DTH, delayed-type hypersensitivity; GEM, gemcitabine; KPS, Karnofsky performance status.

definitive conclusions about clinical efficacy, these findings have been sufficiently encouraging to prompt us to conduct a further clinical study to determine the potency of this combination therapy. No combination chemotherapy, with the exception of FOLFIRINOX,[34] has resulted in a significant improvement in survival of patients with pancreatic cancer although some combination therapies are thought to be more effective for several cancers than single-agent treatments.[1] The use of FOLFIRINOX, however, may have to be limited to patients with good performance status as this regimen has much higher toxicity that sometimes can impair QOL.[34,35] In contrast, as toxicities associated with cancer vaccines are generally mild and acceptable, combination therapies using chemotherapy and cancer vaccine can be expected to exert their clinical benefits without worsening of QOL, which is often impaired by combination chemotherapies using several kinds of cytotoxic agents.

Immunologic monitoring is an important step in the development of evidence-based immunotherapy. Our data provided 2 useful prognostic markers of better clinical outcomes for the combination therapy used in our study. One is DTH to WT1 peptide and the other the frequency of memory-phenotype WT1-CTLs in PB although we did not find the correlation between clinical effects, including survival, and the frequency or absolute numbers of nonphenotypically divided WT1-specific CTLs statistically (data not shown). DTH-positive patients had a notably better prognosis than DTH-negative patients, and the OS curve for DTH-positive

patients showed a late separation beyond the median. As DTH has long been used for evaluation of antigen memory for bacterial, viral, and cancer antigens,[36] the occurrence of DTH to WT1 peptide may reflect the development and persistence of memory-phenotype WT1-CTLs. This can be inferred from our observation that DTH-positive patients showed a significantly higher frequency of memory-phenotype WT1-CTLs than did DTH-negative patients after WT1 vaccination. Furthermore, patients who survived 12 months or longer (superior responders) seemed to have the highest frequency of memory-phenotype WT1-CTLs in their PB although the number of patients in each subgroup was too small to make a statistically valid comparison. It was reported that long-term survivors who had been treated with mutant K-ras vaccine against pancreatic cancer showed the persistence of vaccinated peptide-recognizing T cells (long-term T-cell memory response) for many years after the last vaccination.[37] This report and our results suggest that the development and persistence of TAA-specific CTLs with memory-phenotype resulting from treatment with cancer vaccine contributed to the longer survival. Further investigations are needed to validate these findings in the larger-scale clinical trial.

Despite its potent cytotoxicity, gemcitabine reportedly has immune-modulating functions, such as increase in antigen cross-presentation,[38] and inhibition of B-cells,[39] myeloid-derived suppressive cells,[40] and regulatory T cells,[41] resulting in enhancement of the antigen-specific CTL function. Recently, we reported that gemcitabine enhanced the WT1 expression on human pancreatic cancer cells thus sensitizing the cancer cells to WT1-specific CTL.[11] Furthermore, it was reported that lymphopenia-induced memory-phenotype WT1-CTLs from naive-phenotype WT1-CTLs without self-antigen-induced tolerance.[42] Transient mild to moderate lymphopenia induced by gemcitabine and immediate recovery of T cells could thus promote both the differentiation of naive-phenotype WT1-CTLs into memory-phenotype WT1-CTLs and their proliferation in the clinical application of the combination therapy of gemcitabine and WT1 vaccine. In view of these immunostimulatory properties of gemcitabine, this combination therapy can be expected to generate additional or synergistic effects.

In conclusion, the combination of WT1 vaccine with the standard gemcitabine therapy was well tolerated for patients with advanced pancreatic cancer. WT1 vaccine might have additional effects on gemcitabine to improve survival benefit. An increase in memory-phenotype WT1-CTLs could be a useful predictive marker for a favorable clinical outcome. To determine the clinical efficacy of this combination therapy, we have started a phase 2 randomized clinical study (UMIN000005248).

ACKNOWLEDGMENTS

The authors thank the member of the nursing team for their care for the patients in this trial, Hiroko Nakajima, and Fumihiro Fujiki for their technical supports, Tomoe Umeda for her coordination of clinical research, Takushi Okusaka and Yuji Heike (National Cancer Center in Japan) for their advices about the planning of this study.

CONFLICTS OF INTEREST/ FINANCIAL DISCLOSURES

This study was supported by the Japanese Ministries of Education, Culture, Sports, Science and Technology, and of Health, Labor and Welfare; the National Cancer Center Research and Development Fund; the Takeda Science Foundation; and Mitsui Life Social Welfare Foundation, Promotion of Cancer Research.

All authors have declared there are no financial conflicts of interest with regard to this work.

REFERENCES

1. Stathis A, Moore MJ. Advanced pancreatic carcinoma: current treatment and future challenges. *Nat Rev Clin Oncol.* 2010;7:163–172.
2. Burris HA III, Moore MJ, Andersen J, et al. Improvements in survival and clinical benefit with gemcitabine as first-line therapy for patients with advanced pancreas cancer: a randomized trial. *J Clin Oncol.* 1997;15:2403–2413.
3. Moore MJ, Goldstein D, Hamm J, et al. Erlotinib plus gemcitabine compared with gemcitabine alone in patients with advanced pancreatic cancer: a phase III trial of the National Cancer Institute of Canada Clinical Trials Group. *J Clin Oncol.* 2007;25:1960–1966.
4. Disis ML, Bernhard H, Jaffee EM. Use of tumour-responsive T cells as cancer treatment. *Lancet.* 2009;373:673–683.
5. Mellman I, Coukos G, Dranoff G. Cancer immunotherapy comes of age. *Nature.* 2011;480:480–489.
6. Rosenberg SA, Yang JC, Restifo NP. Cancer immunotherapy: moving beyond current vaccines. *Nat Med.* 2004;10:909–915.
7. Baxevanis CN, Perez SA, Papamichail M. Combinatorial treatments including vaccines, chemotherapy and monoclonal antibodies for cancer therapy. *Cancer Immunol Immunother.* 2009;58:317–324.
8. Nowak AK, Lake RA, Robinson BWS. Combined chemo-immunotherapy of solid tumours: improving vaccines? *Adv Drug Deliv Rev.* 2006;58:975–990.
9. Zitvogel L, Apetoh L, Ghiringhelli F, et al. Immunological aspects of cancer chemotherapy. *Nat Rev Immunol.* 2008;8:59–73.
10. Ramakrishnan R, Assudani D, Nagaraj S, et al. Chemotherapy enhances tumor cell susceptibility to CTL-mediated killing during cancer immunotherapy in mice. *J Clin Invest.* 2010;120:1111–1124.
11. Takahara A, Koido S, Ito M, et al. Gemcitabine enhances Wilms' tumor gene WT1 expression and sensitizes human pancreatic cancer cells with WT1-specific T-cell-mediated antitumor immune response. *Cancer Immunol Immunother.* 2011;60:1289–1297.
12. Huff V. Wilms' tumours: about tumour suppressor genes, an oncogene and a chameleon gene. *Nature Rev Cancer.* 2011;11:111–121.
13. Sugiyama H. WT1 (Wilms' tumor gene 1): biology and cancer immunotherapy. *Jpn J Clin Oncol.* 2010;40:377–387.
14. Elisseeva OA, Oka Y, Tsuboi A, et al. Humoral immune responses against Wilms' tumor gene WT1 product in patients with hematopoietic malignancies. *Blood.* 2002;99:3272–3279.
15. Gaiger A, Carter L, Greinix H, et al. WT1-specific serum antibodies in patients with leukemia. *Clin Cancer Res.* 2001;7:761s–765s.
16. Oji Y, Kitamura Y, Kamino E, et al. WT1 IgG antibody for early detection of nonsmall cell lung cancer and as its prognostic factor. *Int J Cancer.* 2009;125:381–387.
17. Oka Y, Elisseeva OA, Tsuboi A, et al. Human cytotoxic T-lymphocyte responses specific for peptides of the wild-type Wilms' tumor gene (WT1) product. *Immunogenetics.* 2000;51:99–107.
18. Rezvani K, Brenchley JM, Price DA, et al. T-cell responses directed against multiple HLA-A*0201-restricted epitopes derived from Wilms' tumor 1 protein in patients with leukemia and healthy donors: identification, quantification, and characterization. *Clin Cancer Res.* 2005;11:8799–8807.
19. Oka Y, Tsuboi A, Taguchi T, et al. Induction of WT1 (Wilms' tumor gene)-specific cytotoxic T lymphocytes by WT1 peptide vaccine and the resultant cancer regression. *Proc Natl Acad Sci USA.* 2004;101:13885–13890.

20. Morita S, Oka Y, Tsuboi A, et al. A phase I/II trial of a WT1 (Wilms' tumor gene) peptide vaccine in patients with solid malignancy: safety assessment based on the phase I data. *Jpn J Clin Oncol.* 2006;36:231–236.
21. Izumoto S, Tsuboi A, Oka Y, et al. Phase II clinical trial of Wilms tumor 1 peptide vaccination for patients with recurrent glioblastoma multiforme. *J Neurosurg.* 2008;108:963–971.
22. Miyatake T, Ueda Y, Morimoto A, et al. WT1 peptide immunotherapy for gynecologic malignancies resistant to conventional therapies: a phase II trial. *J Cancer Res Clin Oncol.* 2013;139:457–463.
23. Tsuboi A, Oka Y, Kyo T, et al. Long-term WT1 peptide vaccination for patients with acute myeloid leukemia with minimal residual disease. *Leukemia.* 2012;26:1410–1413.
24. Hashii Y, Sato-Miyashita E, Matsumura R, et al. WT1 peptide vaccination following allogeneic stem cell transplantation in pediatric leukemic patients with high risk for relapse: successful maintenance of durable remission. *Leukemia.* 2012; 26:530–532.
25. Keilholz U, Letsch A, Busse A, et al. A clinical and immunologic phase 2 trial of Wilms tumor gene product 1 (WT1) peptide vaccination in patients with AML and MDS. *Blood.* 2009;113:6541–6548.
26. Rezvani K, Yong AS, Mielke S, et al. Leukemia-associated antigen-specific T-cell responses following combined PR1 and WT1 peptide vaccination in patients with myeloid malignancies. *Blood.* 2008;111:236–242.
27. Cella DF, Tulsky DS, Gray G, et al. The functional assessment of cancer therapy scale: development and validation of the general measure. *J Clin Oncol.* 1993;11:570–579.
28. Khorana AA, Fine RL. Pancreatic cancer and thromboembolic disease. *Lancet Oncol.* 2004;5:655–663.
29. Otten HM, Mathijssen J, ten Cate H, et al. Symptomatic venous thromboembolism in cancer patients treated with chemotherapy: an underestimated phenomenon. *Arch Intern Med.* 2004;164:190–194.
30. Okada S, Ueno H, Okusaka T, et al. Phase I trial of gemcitabine in patients with advanced pancreatic cancer. *Jpn J Clin Oncol.* 2001;31:7–12.
31. Gaiger A, Reese V, Disis ML, et al. Immunity to WT1 in the animal model and in patients with acute myeloid leukemia. *Blood.* 2000;96:1480–1489.
32. Gao L, Bellantuono I, Elsasser A, et al. Selective elimination of leukemic CD34 + progenitor cells by cytotoxic T lymphocytes specific for WT1. *Blood.* 2000;95:2198–2203.
33. Ueno H, Ioka T, Ikeda M, et al. Randomized phase III study of gemcitabine plus S-1, S-1 alone, or gemcitabine alone in patients with locally advanced and metastatic pancreatic cancer in Japan and Taiwan: GEST study. *J Clin Oncol.* 2013; 31:1640–1648.
34. Conroy T, Desseigne F, Ychou M, et al. FOLFIRINOX versus gemcitabine for metastatic pancreatic cancer. *N Engl J Med.* 2011;364:1817–1825.
35. Gourgou-Bourgade S, Bascoul-Mollevi C, Desseigne F, et al. Impact of FOLFIRINOX compared with gemcitabine on quality of life in patients with metastatic pancreatic cancer: results from the PRODIGE 4/ACCORD 11 randomized trial. *J Clin Oncol.* 2013;31:23–29.
36. Disis ML. Immunologic biomarkers as correlates of clinical response to cancer immunotherapy. *Cancer Immunol Immunother.* 2011;60:433–442.
37. Wedén S, Klemp M, Gladhaug IP, et al. Long-term follow-up of patients with resected pancreatic cancer following vaccination against mutant K-ras. *Int J Cancer.* 2011;128:1120–1128.
38. Nowak AK, Lake RA, Marzo AL, et al. Induction of tumor cell apoptosis in vivo increases tumor antigen cross-presentation, cross-priming rather than cross-tolerizing host tumor-specific CD8 T cells. *J Immunol.* 2003;170:4905–4913.
39. Nowak AK, Robinson BWS, Lake RA. Gemcitabine exerts a selective effect on the humoral immune response: implications for combination chemo-immunotherapy. *Cancer Res.* 2002;62:2353–2358.
40. Suzuki E, Kapoor V, Jassar AS, et al. Gemcitabine selectively eliminates splenic Gr-1 + /CD11b + myeloid suppressor cells in tumor-bearing animals and enhances antitumor immune activity. *Clin Cancer Res.* 2005;11:6713–6721.
41. Rettig L, Seidenberg S, Parvanova I, et al. Gemcitabine depletes regulatory T-cells in human and mice and enhances triggering of vaccine-specific cytotoxic T-cells. *Int J Cancer.* 2010;129:832–838.
42. Pospori C, Xue SA, Holler A, et al. Specificity for the tumor-associated self-antigen WT1 drives the development of fully functional memory T cells in the absence of vaccination. *Blood.* 2011;117:6813–6824.